

Tuning the valence and concentration of europium and luminescence centers in GaN through co-doping and defect association

Khang Hoang*

Center for Computationally Assisted Science and Technology & Department of Physics,
North Dakota State University, Fargo, North Dakota 58108, United States

(Dated: March 4, 2021)

Defect physics of europium (Eu) doped GaN is investigated using first-principles hybrid density-functional defect calculations. This includes the interaction between the rare-earth dopant and native point defects (Ga and N vacancies) and other impurities (O, Si, C, H, and Mg) unintentionally present or intentionally incorporated into the host material. While the trivalent Eu^{3+} ion is often found to be predominant when Eu is incorporated at the Ga site in wurtzite GaN, the divalent Eu^{2+} is also stable and found to be predominant in a small range of Fermi-level values in the band-gap region. The $\text{Eu}^{2+}/\text{Eu}^{3+}$ ratio can be tuned by tuning the position of Fermi level and through defect association. We find co-doping with oxygen can facilitate the incorporation of Eu into the lattice. The unassociated Eu_{Ga} is an electrically and optically active defect center and its behavior is profoundly impacted by local defect-defect interaction. Defect complexes such as $\text{Eu}_{\text{Ga}}\text{-O}_{\text{N}}$, $\text{Eu}_{\text{Ga}}\text{-Si}_{\text{Ga}}$, $\text{Eu}_{\text{Ga}}\text{-H}_i$, $\text{Eu}_{\text{Ga}}\text{-Mg}_{\text{Ga}}$, and $\text{Eu}_{\text{Ga}}\text{-O}_{\text{N}}\text{-Mg}_{\text{Ga}}$ can efficiently act as deep carrier traps and mediate energy transfer from the host into the Eu^{3+} 4*f*-electron core which then leads to sharp red intra-*f* luminescence. Eu-related defects can also give rise to defect-to-band luminescence. The unassociated Eu_{Ga} , for example, is identified as a possible source of the broad blue emission observed in n-type, Eu^{2+} -containing GaN. This work calls for a re-assessment of certain assumptions regarding specific defect configurations previously made for Eu-doped GaN and further investigation into the origin of the photoluminescence hysteresis observed in (Eu,Mg)-doped samples.

I. INTRODUCTION

Rare-earth (RE) doped III-nitrides are of interest for optoelectronic and spintronic applications [1]. Thanks to their 4*f*-electron core, which is well shielded by the outer $5s^2$ and $5p^6$ electron shells, these RE dopants offer very sharp intra-*f* optical transitions at wavelengths from the infrared to ultraviolet. GaN doped with trivalent europium (Eu^{3+}), for example, emits visible light in the red spectral region and is considered as a promising candidate for light-emitting diodes (LEDs) [2, 3]. In general, a RE luminescence center can be optically excited by resonant (direct) or non-resonant (indirect) excitation. In the former the excitation energy is directly absorbed into the 4*f*-electron core, whereas in the latter it is indirectly transferred from the host. The non-resonant excitation mechanism is believed to be mediated by defects which act as carrier traps; see Fig. 1. An electron (hole) trapped at a defect level can then recombine non-radiatively with a hole (electron) from the valence (conduction) band or some acceptor (donor) level, and the recombination energy is transferred into the 4*f*-core. RE-related defects are of interest in particular because of the close proximity of the RE ion to the carrier trap which enhances energy transfer efficiency. In addition to the intra-*f* luminescence, RE-related defects, like other defects in a semiconductor host, can also act as carrier traps for defect-to-band optical transitions which do not involve energy transfer into the 4*f*-core. A detailed understanding of defect physics in RE-doped semiconduc-

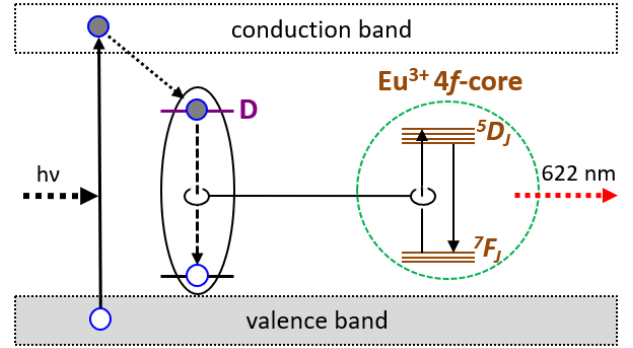


FIG. 1. Schematic illustration of non-resonant Eu^{3+} excitation in GaN. Following a band-to-band excitation of the host, an electron is excited from the valence band to the conduction band. The excited electron is then trapped at the defect level D before recombining non-radiatively with a hole and the recombination energy is transferred into the Eu^{3+} 4*f*-electron core. A mechanism involving hole trapping is similar.

tors is thus essential to understanding their properties and to designing materials with improved performance.

Experimentally, while the trivalent Eu^{3+} ion was found to be predominant in Eu-doped GaN samples and multiple Eu^{3+} luminescence centers were observed [4–12], the divalent Eu^{2+} has also been found or suspected to be present [13–20]. In addition to being of interest for its magnetic properties [14, 15, 20], Eu^{2+} can offer useful luminescence centers in its own right. Mahalingam et al. [18], for example, attributed the broad blue emission in Eu-doped GaN/SiO₂ nanocomposites to the presence of Eu^{2+} . Mitchell et al. [19] reported a thorough work

* khang.hoang@ndsu.edu

on the control of the $\text{Eu}^{2+}/\text{Eu}^{3+}$ ratio in GaN through co-doping and by tuning the growth conditions and were able to achieve high Eu^{2+} concentrations using O and/or Si as co-dopants and suitable experimental conditions. Oxygen was found to play a critical role in the incorporation of Eu into GaN and the quality of Eu-doped GaN samples prepared by organo-metallic vapor phase epitaxy (OMVPE) [19, 21] and lead to sharp and uniform emission spectra and improved energy transfer efficiency [19, 21, 22]. Significant enhancement of the luminescence intensity were also found in GaN co-doped with Eu and Mg [23–27] or Si [28]. Notably, Mg-containing Eu-doped GaN samples were reported to exhibit photoluminescence (PL) hysteresis through the so-called “hysteretic photochromic switching” according to which the observed temperature dependence of PL during a cooling-warming cycle was thought to be due to a switching between two different configurations of an Eu-Mg defect [29–32].

Altogether the luminescence in Eu-doped GaN can be characterized by its complexity with the presence of multiple optically active centers and the dependence on the growth conditions. The interpretation of experimental observations and the discussion in terms of specific defect configurations have been, however, largely speculative.

On the theory side, calculations for Eu-doped GaN were carried out by several research groups using density-functional theory (DFT) based methods, including the local-density approximation (LDA) or self-interaction corrected LDA, the generalized gradient approximation (GGA), and GGA+ U , and LDA+ U within a DFT-based tight-binding approach [33–44]. These studies provided some information on the structural and electronic properties and limited data on defect structure and energetics. Besides, the methods employed in these studies are known to have limited predictive power, especially in determining defect energy levels [45]; see the Supplemental Material (SM) [46] for a detailed discussion. A more rigorous theoretical and computational approach is needed for the study of defect physics in RE-doped semiconductors. In such an approach, the employed methods should possess the ability to overcome the “band-gap problem” encountered in DFT (within LDA or GGA) and DFT+ U calculations and, at the same time, provide a good description of the structural and electronic properties of the RE-doped systems, including local defect structure.

Here, we present a first-principles investigation of defect physics in Eu-doped GaN using hybrid density-functional defect calculations. In these calculations, all orbitals in the material are treated on equal footing, unlike in DFT+ U calculations where the Hubbard U term is applied on the RE $4f$ states only and all other orbitals are left uncorrected. The hybrid DFT/Hartree-Fock method [47] employed here has been shown to be superior to DFT and DFT+ U in the study of defects in semiconductors in general [45] and RE-doped materials in particular [48]. Specific calculations are carried out for the substitutional Eu impurity, native defects (Ga and N vacancies), and impurities (O, Si, C, H, and Mg)

in both the unassociated (i.e., isolated defect) form and the associated (i.e., defect complex) form. These impurities are selected as they are common unintentional or intentional co-dopants in GaN. Based on the results, we discuss the tuning of the valence state and concentration of Eu through co-doping and defect association and examine the role of Eu-related defects as carrier traps for intra- f luminescence and defect-to-band transitions.

II. METHODOLOGY

We model defects in the GaN host using a supercell approach in which a defect is included in a periodically repeated finite volume of the host material. Note that we often use “defect” as a generic term, referring to not only native point defects (intrinsic to the materials) but also impurities (i.e., extrinsic point defects), and defect complexes; impurities can be intentionally incorporated (i.e., dopants) or unintentionally present. The formation energy of a defect X in effective charge state q (i.e., with respect to the host lattice) is defined as [45, 49]

$$E^f(X^q) = E_{\text{tot}}(X^q) - E_{\text{tot}}(\text{bulk}) - \sum_i n_i \mu_i + q(E_v + \mu_e) + \Delta^q, \quad (1)$$

where $E_{\text{tot}}(X^q)$ and $E_{\text{tot}}(\text{bulk})$ are the total energies of the defect and bulk supercells; n_i is the number of atoms of species i that have been added ($n_i > 0$) or removed ($n_i < 0$) to form the defect; μ_i is the atomic chemical potential, representing the energy of the reservoir with which atoms are being exchanged. μ_e is the electronic chemical potential, i.e., the Fermi level, representing the energy of the electron reservoir, referenced to the valence-band maximum (VBM) in the bulk (E_v). Finally, Δ^q is the correction term to align the electrostatic potentials of the bulk and defect supercells and to account for finite-size effects on the total energies of charged defects, calculated following the procedure of Freysodt et al. [50, 51].

In thermodynamic *equilibrium*, the formation energy of a defect directly determines the concentration [49]:

$$c = N_{\text{sites}} N_{\text{config}} \exp\left(\frac{-E^f}{k_B T}\right), \quad (2)$$

where N_{sites} is the number of high-symmetry sites in the lattice (per unit volume) on which the defect can be incorporated, N_{config} is the number of equivalent configurations (per site), and k_B is the Boltzmann constant. Clearly, at a given temperature, a defect that has a lower formation energy will be more likely to form and occur with a higher concentration. Note that, when a material is prepared under *non-equilibrium* conditions, excess defects can be frozen-in and the equilibrium concentration estimated via Eq. (2) is only the *lower bound* [52].

While the Fermi level in Eq. (1) can be treated as a variable, it is not a free parameter. The actual Fermi-

level position can be determined by solving the charge-neutrality equation [49]:

$$\sum_i c_i q_i - n_e + n_h = 0, \quad (3)$$

where c_i and q_i are the concentration and charge, respectively, of defect X_i ; n_e and n_h are free electron and hole concentrations, respectively; and the summation is over all possible defects present in the material

From defect formation energies, one can calculate the *thermodynamic* transition level between charge states q and q' of a defect, $\epsilon(q/q')$, defined as the Fermi-level position at which the formation energy of the defect in charge state q is equal to that in charge state q' [45], i.e.,

$$\epsilon(q/q') = \frac{E^f(X^q; \mu_e = 0) - E^f(X^{q'}; \mu_e = 0)}{q' - q}, \quad (4)$$

where $E^f(X^q; \mu_e = 0)$ is the formation energy of the defect X in charge state q when the Fermi level is at the VBM ($\mu_e = 0$). This $\epsilon(q/q')$ level [often referred to as the (q/q') level], corresponding to a *defect energy level* (or simply *defect level*), would be observed in, e.g., deep-level transient spectroscopy (DLTS) experiments where the defect in the final charge state q' fully relaxes to its equilibrium configuration after the transition. Note that these defect levels are *not* the same as the Kohn-Sham levels obtained in a band-structure calculation such as those associated with the so-called “defect states” that may be observed in the electronic density of states (DOS) of a system in the presence of a defect. Strictly speaking, the Kohn-Sham levels cannot be directly identified with any levels that can be observed in experiments [45, 49].

The *optical* transition level $E_{\text{opt}}^{q/q'}$ is defined similarly but with the total energy of the final state q' calculated using the lattice configuration of the initial state q [45].

Our total-energy calculations are based on DFT with the Heyd-Scuseria-Ernzerhof (HSE) functional [47], the projector augmented wave method [53], and a plane-wave basis set, as implemented in the Vienna *Ab Initio* Simulation Package (VASP) [54]. Along with the CPU version, the graphics processing unit (GPU) port [55, 56] of VASP is also used. The Hartree-Fock mixing parameter is set to 0.31 and the screening length to the default value of 10 Å. These parameters result in a band gap of 3.53 eV for GaN, very close to that (~ 3.5 eV) reported in experiments. Defects in GaN are simulated using a 96-atom supercell and a $2 \times 2 \times 2$ Monkhorst-Pack k -point mesh for the integrations over the Brillouin zone. In defect calculations, the lattice parameters are fixed to the calculated bulk values but all the internal coordinates are relaxed. The Eu 4*f* electrons are included explicitly in the calculations since in Eu-doped GaN the 4*f* states are present in the band gap and play an important role in defect formation (This is different from, e.g., the case of erbium (Er) doped GaN in which Er 4*f* electrons can be included in the core [57]). The Ga 3*d* electrons are treated as core states as the inclusion of these electrons in the valence

has small effects on the defect transition level; see the SM [46] for more details. In all calculations, the plane-wave basis-set cutoff is set to 400 eV and spin polarization is included. All structural relaxations are performed with HSE and the force threshold is chosen to be 0.04 eV/Å or smaller. Spin-orbit coupling (SOC) is not included since significant cancellation is expected between the terms in Eqs. (1) and (4). Our tests show that the $\epsilon(0/-)$ level of Eu_{Ga} obtained in HSE+SOC calculations is different from that obtained in HSE calculations by only 7 meV.

The chemical potentials of Ga, N, Eu, H, C, O, Si, and Mg are referenced to the total energy per atom of bulk Ga, N_2 at 0 K, bulk Eu, H_2 at 0 K, bulk C (diamond), O_2 at 0 K, bulk Si, and bulk Mg, respectively. μ_{Ga} and μ_{N} vary over a range determined by the formation enthalpy of GaN such that $\mu_{\text{Ga}} + \mu_{\text{N}} = \Delta H(\text{GaN})$ (calculated to be -1.26 eV at 0 K). We will examine defect landscape in GaN in two extreme limits: Ga-rich ($\mu_{\text{Ga}} = 0$) and N-rich ($\mu_{\text{N}} = 0$) conditions. Specific values of the Eu, H, C, O, Si, and Mg chemical potentials are determined by assuming equilibrium with EuN ($\Delta H = -1.20$ eV at 0 K), H_2 at 0 K, bulk C, $\beta\text{-Ga}_2\text{O}_3$ (-10.07 eV), $\beta\text{-Si}_3\text{N}_4$ (-9.17 eV), and Mg_3N_2 (-4.16 eV), respectively. Note that the transition levels $\epsilon(q/q')$ and $E_{\text{opt}}^{q/q'}$ are *independent* of the choice of the atomic chemical potentials.

III. RESULTS

A. Unassociated native defects and impurities

In bulk (i.e., perfect and undoped) GaN (wurtzite, space group $P6_3mc$), each Ga is coordinated with four N atoms: one along the c -axis and three in the basal (ab) plane. There is a small C_{3v} distortion at the Ga lattice site with the Ga–N bond length calculated for the axial N atom (1.958 Å) slightly different from that for the basal N atoms (1.952 Å). For comparison, the experimental values for the axial and basal Ga–N bond lengths are 1.956 Å and 1.949 Å [58], respectively. In the presence of a defect, the lattice environment in the defect’s vicinity can be further distorted, and such a local distortion is often different for different charge configurations.

Figure 2 shows the formation energies of various *unassociated* native defects and impurities in GaN. The substitutional Eu impurity (Eu_{Ga}) is found to be stable as Eu_{Ga}^0 (i.e., Eu^{3+} at the Ga^{3+} lattice site, with a calculated magnetic moment of 6 μ_{B} ; spin $S = 3$) and/or Eu_{Ga}^- (i.e., Eu^{2+} at the Ga^{3+} site, with a magnetic moment of 7 μ_{B} ; spin $S = 7/2$), depending on the Fermi-level position. Eu_{Ga} introduces two defect levels in the host band gap: the $(+/0)$ level at 0.22 eV above the VBM and the $(0/-)$ level at 3.09 eV (i.e., 0.44 eV below the CBM). Note, however, that “ Eu_{Ga}^+ ” is not a true charge state of Eu_{Ga} . It is, in fact, a defect complex consisting of Eu_{Ga}^0 and an electron hole (h^* ; spin $S = 1/2$) *localized* on one of the neighboring basal N atoms. In the Eu_{Ga}^0 (Eu_{Ga}^-) configuration, the Eu–N bond length is 2.233 Å (2.321

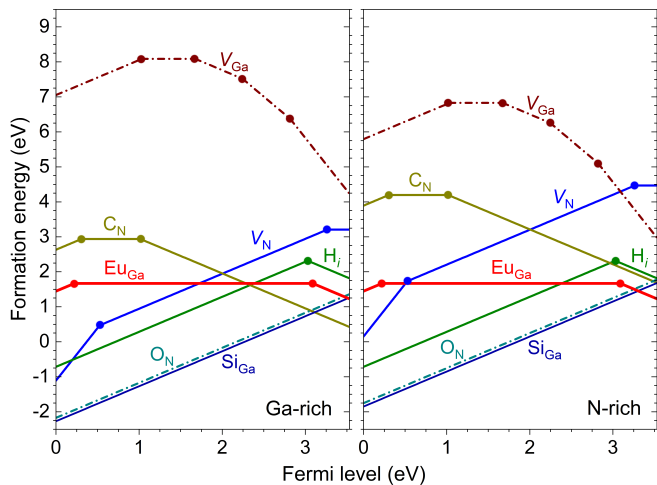


FIG. 2. Formation energies of Eu_{Ga} and relevant native point defects (V_{N} , V_{Ga}) and impurities (H_i , C_{N} , O_{N} , Si_{Ga}) in GaN, plotted as a function of Fermi level from the VBM (at 0 eV) to the conduction-band minimum (CBM, at 3.53 eV), under the extreme Ga-rich and N-rich conditions. For each defect, only segments corresponding to the lowest-energy charge states are shown. The slope of these segments indicates the charge state [i.e., q in Eq. (1)]: positively (negatively) charged defect configurations have positive (negative) slopes; horizontal segments correspond to neutral defect configurations. Large solid dots connecting two segments with different slopes, if present, mark the *defect levels* [i.e., the thermodynamic transition levels, $\epsilon(q/q')$, calculated according to Eq. (4)].

Å) for the axial N atom and 2.197–2.208 Å (2.283–2.297 Å) for the basal N atoms. The local distortion at the Ga lattice site where the Eu dopant is incorporated is thus more pronounced and slightly deviates from the C_{3v} symmetry. The result is also consistent with the fact that the ionic radius of Eu^{3+} is smaller than that of Eu^{2+} .

The electronic behavior of Eu is thus different from that of, e.g., erbium (Er) in GaN. Er was found to be stable only as Er^{3+} , and the unassociated Er_{Ga} does not introduce any defect levels [57]. The origin of the difference can be traced back to the difference in their electronic structure: Eu introduces an unoccupied $4f$ state in the host band gap, whereas Er does not produce any in-gap $4f$ state; see the SM [46] for a detailed analysis of the electronic structure of Eu- *vs.* Er-doped GaN obtained in DFT+ U and HSE calculations. As a result, upon adding an electron to Eu_{Ga}^0 to form Eu_{Ga}^- the extra electron goes to the lowest unoccupied state (in this case, the in-gap Eu $4f$ state), leading to the valence change from Eu^{3+} to Eu^{2+} ; see Fig. 4 of the SM [46]. In the case of Er, the extra electron goes to the CBM (composed of the host states) and becomes delocalized; the valence change, therefore, does not occur and “ Er_{Ga}^- ” cannot be stabilized [57]. The implications of the $(0/-)$ level of Eu_{Ga} and the valence change are discussed in Sec. IV.

Our result for Eu_{Ga} is *significantly* different from that previously reported in the literature [33–35]. Filhol et

al. [33] and Svane et al. [34] did not find any defect energy level in the calculated band gap, i.e., Eu is stable as Eu^{3+} in the entire range of the Fermi-level values from the VBM to the CBM, which is in contrast to the fact that Eu^{2+} is also stable in GaN. Sanna et al. [35], on the other hand, reported the $(0/-)$ level of Eu_{Ga} to be at 1.58 eV above the VBM, which is about 1.5 eV lower than that found in our calculations. A more detailed discussion of those previous studies is provided in the SM [46].

The results for the nitrogen vacancy (V_{N}), gallium vacancy (V_{Ga}), hydrogen interstitial (H_i), and substitutional carbon (C_{N}) and oxygen (O_{N}) were already reported and discussed in detail in Ref. [57] but are included in Fig. 2 for easy reference since in the next sections we will discuss defect complexes consisting of Eu_{Ga} and these native point defects and impurities. V_{N} introduces the $(3+/+)$ level at 0.53 eV above the VBM and the $(+/0)$ level at 0.27 eV below the CBM. V_{Ga} has four defect levels in the band gap: $(+/0)$ at 1.03 eV and $(0/-)$ at 1.67 eV above the VBM, and $(-2-)$ at 1.29 eV and $(2-/3-)$ at 0.71 eV below the CBM. H_i is amphoteric [i.e., positively (negatively) charged in the p -type (n -type) GaN] and its $(+/-)$ level occurs at 0.50 eV below the CBM. C_{N} has two defect levels: $(+/0)$ at 0.31 eV and $(0/-)$ at 1.02 eV above the VBM. O_{N} is a shallow donor and only stable as O_{N}^+ [57]. We find that Si_{Ga} is also a shallow donor, being stable only in the Si_{Ga}^+ configuration. Si (O) thus readily donates one electron to the lattice and becomes a positively charged defect when incorporated at the Ga (N) lattice site in GaN. The result for Si_{Ga} is in agreement with that previously reported by other groups [59–61].

B. Defect complexes of Eu and native defects

Some of the unassociated defects discussed in Sec. III A can come close and form complexes. Such defect association often changes the local lattice environment and defect energetics and can lead to important implications. Among possible complexes between Eu_{Ga} and native defects, $\text{Eu}_{\text{Ga}}-V_{\text{N}}$ and $\text{Eu}_{\text{Ga}}-V_{\text{Ga}}$ have been widely thought to be possible defect centers for intra- f luminescence in Eu-doped GaN [2, 3, 5, 11, 37]. Figure 3 shows the formation energies of these complexes. In $\text{Eu}_{\text{Ga}}-V_{\text{N}}$, the V_{N} part can be at the basal or axial lattice site with respect to Eu_{Ga} ; see Fig. 4. We find that $\text{Eu}_{\text{Ga}}-(V_{\text{N}})_{\text{basal}}$ introduces four defect levels in the band gap region: $(3+/2+)$ at 0.48 eV, $(2+/+)$ at 1.18 eV, and $(+/0)$ at 1.86 eV above the VBM, and $(0/-)$ at 0.07 eV above the CBM. A careful inspection shows that in going from $(\text{Eu}_{\text{Ga}}-V_{\text{N}})^0$ to $(\text{Eu}_{\text{Ga}}-V_{\text{N}})^-$ the additional electron stays in the vicinity of the void formed by V_{N} ; $(\text{Eu}_{\text{Ga}}-V_{\text{N}})^0$ is a defect complex consisting of Eu_{Ga}^- and V_{N}^+ whereas $(\text{Eu}_{\text{Ga}}-V_{\text{N}})^-$ is a complex of Eu_{Ga}^- and V_{N}^0 ; see also Table I. The extra electron is thus captured by the V_{N} part of the complex and Eu at the Ga site remains Eu^{2+} . The axial geometric configuration, i.e., $\text{Eu}_{\text{Ga}}-(V_{\text{N}})_{\text{axial}}$, has a higher formation energy than the basal one in all the stable charge states;

TABLE I. Eu-related defects in Eu-doped GaN: The stable valence state of the rare-earth (RE) ion, constituent defects, binding energy (E_b , with respect to the isolated constituents), magnetic moment (M), and defect levels [$\epsilon(q/q')$, with respect to the VBM (E_v , at 0 eV) or the CBM (E_c , at 3.53 eV)]. Note that h^* is an electron hole localized at an N lattice site. Spin-polarized defects in a complex are found to interact ferromagnetically; the magnetic moment of the complex is thus equal to the sum of those of the constituents. The values in the parentheses are for the axial (with respect to Eu) configurations.

Defect	RE ion	Constituents	E_b (eV)	M (μ_B)	Defect levels (eV)
Eu_{Ga}^+	Eu^{3+}	$\text{Eu}_{\text{Ga}}^0 + h^*$		7	$\epsilon(+/0) = E_v + 0.22$
Eu_{Ga}^0	Eu^{3+}	Eu_{Ga}^0		6	$\epsilon(0/-) = E_c - 0.44$
Eu_{Ga}^-	Eu^{2+}	Eu_{Ga}^-		7	
$(\text{Eu}_{\text{Ga}}-\text{V}_{\text{N}})^{3+}$	Eu^{3+}	$\text{Eu}_{\text{Ga}}^0 + \text{V}_{\text{N}}^{3+}$	1.58 (1.11)	6	$\epsilon(3+ / 2+) = E_v + 0.48$ (0.42)
$(\text{Eu}_{\text{Ga}}-\text{V}_{\text{N}})^{2+}$	$\text{Eu}^{2+(3+)}$	$\text{Eu}_{\text{Ga}}^{-(0)} + \text{V}_{\text{N}}^{3+(2+)}$	4.18 (1.25)	7	$\epsilon(2+ / +) = E_v + 1.18$ (0.99)
$(\text{Eu}_{\text{Ga}}-\text{V}_{\text{N}})^+$	Eu^{3+}	$\text{Eu}_{\text{Ga}}^0 + \text{V}_{\text{N}}^+$	0.97 (0.75)	6	$\epsilon(+/0) = E_c - 1.67$ (1.65)
$(\text{Eu}_{\text{Ga}}-\text{V}_{\text{N}})^0$	Eu^{2+}	$\text{Eu}_{\text{Ga}}^0 + \text{V}_{\text{N}}^+$	2.20 (1.96)	7	$\epsilon(0/-) = E_c + 0.07$ (0.03)
$(\text{Eu}_{\text{Ga}}-\text{V}_{\text{N}})^-$	Eu^{2+}	$\text{Eu}_{\text{Ga}}^- + \text{V}_{\text{N}}^0$	1.86 (1.67)	8	
$(\text{Eu}_{\text{Ga}}-\text{V}_{\text{Ga}})^{3+}$	Eu^{3+}			6	$\epsilon(3+ / 2+) = E_v + 0.87$
$(\text{Eu}_{\text{Ga}}-\text{V}_{\text{Ga}})^{2+}$	Eu^{3+}			7	$\epsilon(2+ / +) = E_v + 1.23$
$(\text{Eu}_{\text{Ga}}-\text{V}_{\text{Ga}})^+$	Eu^{2+}			8	$\epsilon(+/0) = E_v + 2.06$
$(\text{Eu}_{\text{Ga}}-\text{V}_{\text{Ga}})^0$	Eu^{2+}			9	$\epsilon(0/-) = E_c - 1.38$
$(\text{Eu}_{\text{Ga}}-\text{V}_{\text{Ga}})^-$	Eu^{3+}	$\text{Eu}_{\text{Ga}}^0 + \text{V}_{\text{Ga}}^-$	0.18	8	$\epsilon(-/2-) = E_c - 1.34$
$(\text{Eu}_{\text{Ga}}-\text{V}_{\text{Ga}})^{2-}$	Eu^{3+}	$\text{Eu}_{\text{Ga}}^0 + \text{V}_{\text{Ga}}^{2-}$	0.23	7	$\epsilon(2- / 3-) = E_c - 0.92$
$(\text{Eu}_{\text{Ga}}-\text{V}_{\text{Ga}})^{3-}$	Eu^{3+}	$\text{Eu}_{\text{Ga}}^0 + \text{V}_{\text{Ga}}^{3-}$	0.45	6	
$(\text{Eu}_{\text{Ga}}-\text{H}_i)^+$	Eu^{3+}	$\text{Eu}_{\text{Ga}}^0 + \text{H}_i^+$	1.25	6	$\epsilon(+/0) = E_c - 1.36$
$(\text{Eu}_{\text{Ga}}-\text{H}_i)^0$	Eu^{2+}	$\text{Eu}_{\text{Ga}}^- + \text{H}_i^+$	2.17	7	
$(\text{Eu}_{\text{Ga}}-\text{C}_{\text{N}})^+$	Eu^{3+}	$\text{Eu}_{\text{Ga}}^0 + \text{C}_{\text{N}}^+$	0.61 (0.50)	8	$\epsilon(+/0) = E_v + 0.33$ (0.17)
$(\text{Eu}_{\text{Ga}}-\text{C}_{\text{N}})^0$	Eu^{3+}	$\text{Eu}_{\text{Ga}}^0 + \text{C}_{\text{N}}^0$	0.58 (0.63)	7	$\epsilon(0/-) = E_c - 1.08$ (1.17)
$(\text{Eu}_{\text{Ga}}-\text{C}_{\text{N}})^-$	Eu^{3+}	$\text{Eu}_{\text{Ga}}^0 + \text{C}_{\text{N}}^-$	-0.86 (-0.71)	6	
$(\text{Eu}_{\text{Ga}}-\text{O}_{\text{N}})^+$	Eu^{3+}	$\text{Eu}_{\text{Ga}}^0 + \text{O}_{\text{N}}^+$	0.76 (0.62)	6	$\epsilon(+/0) = E_c - 1.26$ (1.23)
$(\text{Eu}_{\text{Ga}}-\text{O}_{\text{N}})^0$	Eu^{2+}	$\text{Eu}_{\text{Ga}}^0 + \text{O}_{\text{N}}^+$	1.59 (1.41)	7	
$(\text{Eu}_{\text{Ga}}-\text{Si}_{\text{Ga}})^+$	Eu^{3+}	$\text{Eu}_{\text{Ga}}^0 + \text{Si}_{\text{Ga}}^+$	0.32	6	$\epsilon(+/0) = E_c - 1.04$
$(\text{Eu}_{\text{Ga}}-\text{Si}_{\text{Ga}})^0$	Eu^{2+}	$\text{Eu}_{\text{Ga}}^- + \text{Si}_{\text{Ga}}^+$	0.92	7	
$(\text{Eu}_{\text{Ga}}-\text{Mg}_{\text{Ga}})^0$	Eu^{3+}	$\text{Eu}_{\text{Ga}}^0 + \text{Mg}_{\text{Ga}}^- + h^*$	0.48 (0.40) ^a	7	$\epsilon(0/-) = E_v + 0.97$ (0.85)
$(\text{Eu}_{\text{Ga}}-\text{Mg}_{\text{Ga}})^-$	Eu^{3+}	$\text{Eu}_{\text{Ga}}^0 + \text{Mg}_{\text{Ga}}^-$	-0.10 (-0.06)	6	
$(\text{Eu}_{\text{Ga}}-\text{O}_{\text{N}}-\text{Mg}_{\text{Ga}})^0$	Eu^{3+}	$\text{Eu}_{\text{Ga}}^0 + \text{O}_{\text{N}}^+ + \text{Mg}_{\text{Ga}}^-$	1.70	6	$\epsilon(0/-) = E_c - 0.78$
$(\text{Eu}_{\text{Ga}}-\text{O}_{\text{N}}-\text{Mg}_{\text{Ga}})^-$	Eu^{2+}	$\text{Eu}_{\text{Ga}}^0 + \text{O}_{\text{N}}^+ + \text{Mg}_{\text{Ga}}^-$	2.04	7	

^aWith respect to Eu_{Ga}^0 and “ Mg_{Ga}^0 ”.

its defect transition levels are also slightly shifted as seen in Fig. 3; e.g., the (0/-) level is now at 0.03 eV above the CBM. $\text{Eu}_{\text{Ga}}-\text{V}_{\text{Ga}}$, on the other hand, has six defect levels in the host band gap: (3+ / 2+) at 0.87 eV, (2+ / +) at 1.23 eV, (+/0) at 2.06 eV, (0/-) at 2.15 eV, (-/2-) at 2.19 eV, and (2- / 3-) at 2.61 eV above the VBM.

The local lattice environment is changed significantly due to defect-defect interaction. In $(\text{Eu}_{\text{Ga}}-\text{V}_{\text{N}})^0$, for example, Eu moves off-center and closer to the vacancy by 0.27 Å; see Fig. 4(a). The binding energy of the complex with respect to its isolated constituents, Eu_{Ga}^- and V_{N}^+ ,

is 2.20 eV. In the other stable charge states of the basal configuration, $(\text{Eu}_{\text{Ga}}-\text{V}_{\text{N}})^q$ with $q = +, 2+,$ and $3+,$ the displacement is 0.19 Å, 0.58 Å, and 0.38 Å, respectively. Similar distortion is observed in the axial geometric configurations; e.g., the displacement of Eu in $(\text{Eu}_{\text{Ga}}-\text{V}_{\text{N}})^0$ is 0.25 Å along the c -axis and toward the vacancy; see Fig. 4(b). Note that there is significant difference between the basal and axial configurations in the case of $(\text{Eu}_{\text{Ga}}-\text{V}_{\text{N}})^{2+}$ where Eu is stable as Eu^{2+} in the former and as Eu^{3+} in the latter; see more details in the SM [46]. The local distortion is generally larger in $(\text{Eu}_{\text{Ga}}-$

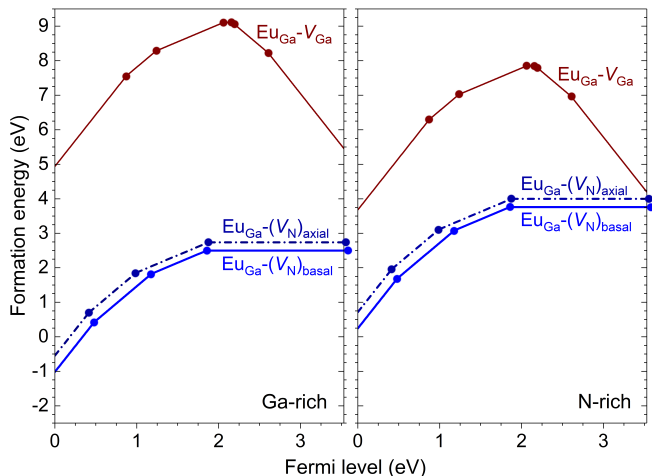


FIG. 3. Formation energies of defect complexes consisting of Eu_{Ga} and native defects in GaN, $\text{Eu}_{\text{Ga}}\text{-V}_{\text{N}}$ and $\text{Eu}_{\text{Ga}}\text{-V}_{\text{Ga}}$, plotted as a function of Fermi level from the VBM to the CBM, under the Ga-rich and N-rich conditions. For each defect, only segments corresponding to the lowest-energy charge states are shown. Large solid dots connecting two segments with different slopes mark the defect levels. V_{N} can be at the basal or axial N site with respect to the Eu_{Ga} component. The $(0/-)$ level of $\text{Eu}_{\text{Ga}}\text{-V}_{\text{N}}$ is right above the CBM.

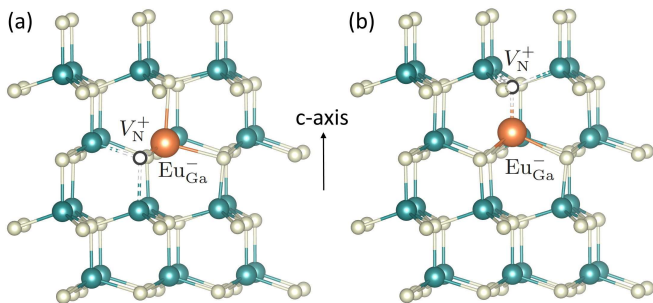


FIG. 4. Structure of $(\text{Eu}_{\text{Ga}}\text{-V}_{\text{N}})^0$: (a) basal and (b) axial geometric configurations. Large spheres are Eu, medium Ga, small N. The nitrogen vacancy is represented by a black circle.

$\text{V}_{\text{Ga}})^q$ where Eu moves off-center by 0.80 \AA ($q = 0$), 0.34 \AA ($-$), 0.49 \AA ($2-$), and 1.33 \AA ($3-$). The position of their neighboring atoms is also shifted; see Figs. 4 and 5.

The structure and energetics of a defect complex, in general, can be expressed in terms of those of its isolated constituents which are usually elementary defects acting as basic building blocks [62, 63]. The example involving $\text{Eu}_{\text{Ga}}\text{-V}_{\text{N}}$ given above is an illustration of such an analysis which is key to understanding complex defect configurations. In Table I, we list the characteristics of all Eu-related defect complex configurations, including the valence state of Eu, constituent defects, and binding energy of the complexes with respect to the isolated constituents. Note that the decomposition of $(\text{Eu}_{\text{Ga}}\text{-V}_{\text{Ga}})^q$ with $q = 0, +, 2+, 3+$ into basic building blocks is not straightforward due to strong lattice distortion, involv-

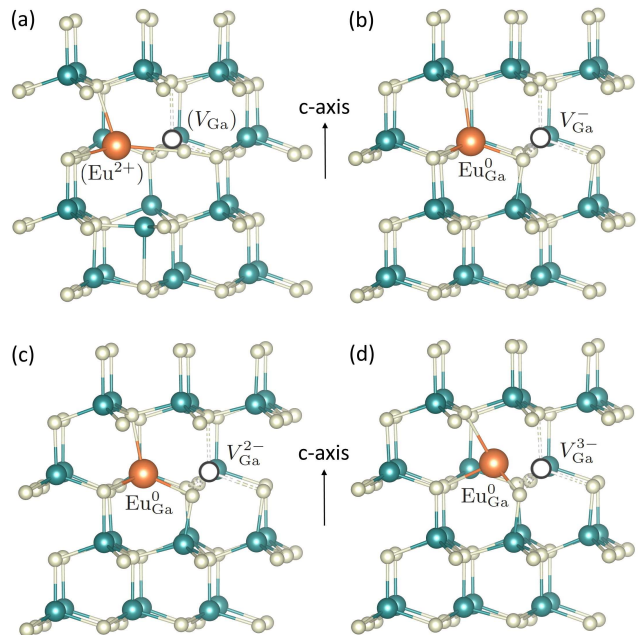


FIG. 5. Structure of representative $(\text{Eu}_{\text{Ga}}\text{-V}_{\text{Ga}})^q$ defect configurations: (a) $q = 0$, (b) $q = -$, (c) $q = 2-$, and (d) $q = 3-$. Large spheres are Eu, medium Ga, and small N. The gallium vacancy is represented by a black circle. The structures associated with $q = +, 2+, 3+$ (not shown here) are similar to that of $q = 0$. In (a), the charge state of the V_{Ga} constituent cannot be clearly determined at this point; see the text.

ing not just Eu but also Ga and N atoms, which makes it difficult to clearly identify constituent defects.

The results summarized in Table I show that Eu is stable as Eu^{3+} or Eu^{2+} in $\text{Eu}_{\text{Ga}}\text{-V}_{\text{N}}$ and $\text{Eu}_{\text{Ga}}\text{-V}_{\text{Ga}}$, depending on specific charge states. Compared to the unassociated Eu_{Ga} , the association between Eu_{Ga} and V_{N} is found to extend the range of Fermi-level values below the CBM in which Eu^{2+} is energetically more stable than Eu^{3+} . This is due to the strong Coulomb attraction between Eu_{Ga}^- and V_{N}^+ in $(\text{Eu}_{\text{Ga}}\text{-V}_{\text{N}})^0$, which leads to a larger reduction (due to defect association) in the formation energy of the neutral charge state compared to that of the preceding ($+$) and subsequent ($-$) stable charge states, as reflected in the binding energies reported in Table I. As a result, the $(+/0)$ level of $\text{Eu}_{\text{Ga}}\text{-V}_{\text{N}}$ is shifted toward the VBM and the $(0/-)$ level toward the CBM, compared to those of the unassociated Eu_{Ga} , thus extending the stability range of $(\text{Eu}_{\text{Ga}}\text{-V}_{\text{N}})^0$ and hence Eu^{2+} ; see Fig. 3. The basal configuration of $(\text{Eu}_{\text{Ga}}\text{-V}_{\text{N}})^{2+}$, discussed earlier and in the SM [46], presents an even more interesting case where Eu^{2+} can be stabilized far from the CBM. In this example, the strong local elastic and electrostatic interactions play a key role in stabilizing Eu_{Ga}^- and V_{N}^{3+} and in lowering the complex's formation energy.

The binding energy of $\text{Eu}_{\text{Ga}}\text{-V}_{\text{N}}$ is relatively large, suggesting that it can exist as a defect complex in real samples. $\text{Eu}_{\text{Ga}}\text{-V}_{\text{Ga}}$, on the other hand, has a much smaller

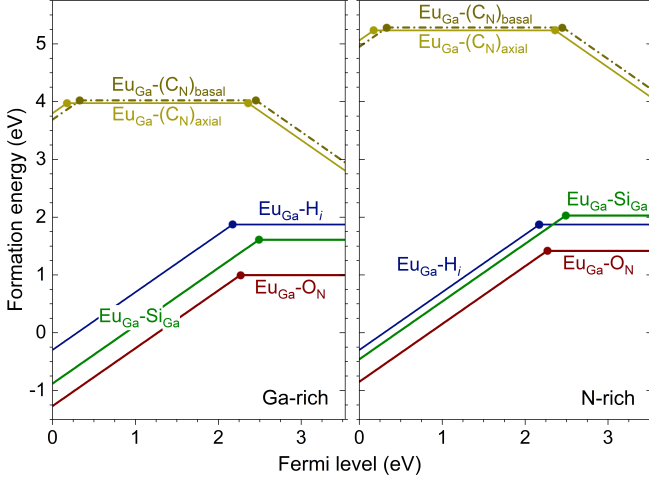


FIG. 6. Formation energies of defect complexes consisting of Eu_{Ga} and impurities in GaN, $\text{Eu}_{\text{Ga}}\text{-H}_i$, $\text{Eu}_{\text{Ga}}\text{-C}_N$, $\text{Eu}_{\text{Ga}}\text{-O}_N$, and $\text{Eu}_{\text{Ga}}\text{-Si}_{\text{Ga}}$, plotted as a function of Fermi level from the VBM to the CBM, under the Ga-rich and N-rich conditions. For each defect, only segments corresponding to the lowest-energy charge states are shown. Large solid dots connecting two segments with different slopes mark the defect levels. C_N can be at the basal or axial N site with respect to Eu_{Ga} . Only the basal configuration if $\text{Eu}_{\text{Ga}}\text{-O}_N$ is included.

binding energy; see Table I. Together with the high calculated formation energy (Fig. 3), $\text{Eu}_{\text{Ga}}\text{-V}_{\text{Ga}}$ is unlikely to be stable or occur with a high concentration as a complex under thermodynamic equilibrium growth conditions. It is more likely to be created under non-equilibrium conditions such as during Eu implantation. The same can be said about $\text{Eu}_{\text{Ga}}\text{-V}_N$ whose formation energy is high under n -type conditions; see Fig. 3.

The electronic behavior of $\text{Eu}_{\text{Ga}}\text{-V}_N$ is similar to $\text{Er}_{\text{Ga}}\text{-V}_N$ in GaN. $\text{Er}_{\text{Ga}}\text{-(V}_N\text{)}_{\text{basal}}$ was reported to also have the $(0/-)$ level at 0.02 eV above the CBM [57]. Our results for $\text{Eu}_{\text{Ga}}\text{-V}_N$ and $\text{Eu}_{\text{Ga}}\text{-V}_{\text{Ga}}$ are, however, *qualitatively* different from those reported by other groups [33, 35, 36]; see the SM [46] for a detailed discussion and comparison.

C. Defect complexes of Eu and other impurities

In addition to the native defects, Eu_{Ga} can also form complexes with impurities that are unintentionally present in the growth environment or intentionally incorporated into the host material as co-dopants. Figure 6 shows the formation energies of defect complexes $\text{Eu}_{\text{Ga}}\text{-H}_i$, $\text{Eu}_{\text{Ga}}\text{-C}_N$, $\text{Eu}_{\text{Ga}}\text{-O}_N$, and $\text{Eu}_{\text{Ga}}\text{-Si}_{\text{Ga}}$. $\text{Eu}_{\text{Ga}}\text{-H}_i$ has one defect level in the bulk band gap: $(+/0)$ at 1.36 eV below the CBM. The $(\text{Eu}_{\text{Ga}}\text{-H}_i)^0$ configuration is a defect complex consisting of Eu_{Ga}^0 and H_i^+ , whereas $(\text{Eu}_{\text{Ga}}\text{-H}_i)^+$ is a complex of Eu_{Ga}^+ and H_i^+ ; see also Table I. The valence state of Eu in the complex thus changes as one crosses the transition level $\epsilon(+/0)$. In these defect com-

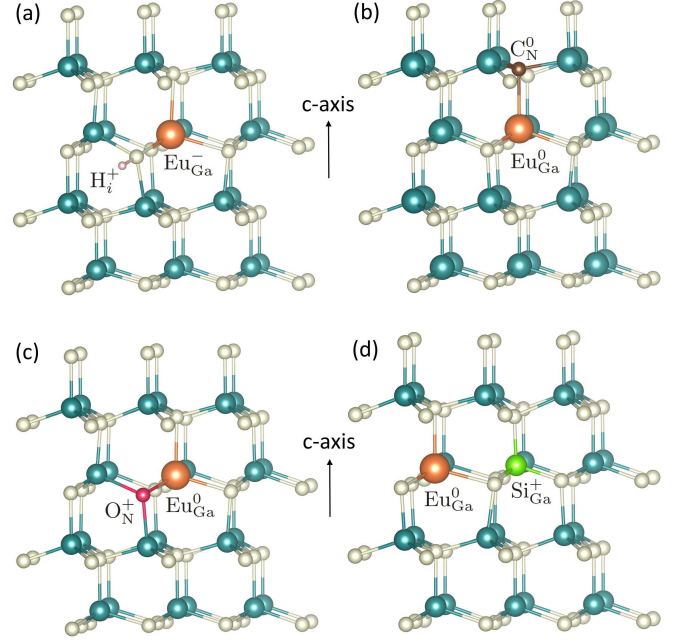


FIG. 7. Structure of (a) $(\text{Eu}_{\text{Ga}}\text{-H}_i)^0$, (b) $(\text{Eu}_{\text{Ga}}\text{-C}_N)^0$, (c) $(\text{Eu}_{\text{Ga}}\text{-O}_N)^+$, and (d) $(\text{Eu}_{\text{Ga}}\text{-Si}_{\text{Ga}})^+$ complexes. Large spheres are Eu, medium Ga/Si, small N/C/O, and smallest H.

plexes, the H interstitial is bonded to one of the nearest N neighbors of Eu. In $(\text{Eu}_{\text{Ga}}\text{-H}_i)^{0(+)}$, the N-H distance is 1.00 Å (1.02 Å) and the distance between Eu and the N atom in the NH unit is 2.34 Å (2.30 Å); see Fig. 7(a).

$\text{Eu}_{\text{Ga}}\text{-C}_N$ has two geometric configurations associated with two possible positions of C_N with respect to Eu_{Ga} . $\text{Eu}_{\text{Ga}}\text{-C}_N$ introduces two defect levels: $(+/0)$ at 0.33 eV (0.17 eV) above the VBM and $(0/-)$ at 1.08 eV (1.17 eV) below the CBM for the basal (axial) configuration. The distance between the two defects in the complex is 2.27 Å, 2.35 Å, or 2.23 Å for the 0, +, or - charge state, respectively; see Fig. 7(b). $(\text{Eu}_{\text{Ga}}\text{-C}_N)^-$ has a negative binding energy and is thus unstable toward its isolated constituents, Eu_{Ga}^0 and C_N^- . In other words, $\text{Eu}_{\text{Ga}}\text{-C}_N$ is unlikely to be stable as a defect complex when incorporated under n -type conditions. The other stable charge states of the defect complex have positive but small binding energies; see Table I. A combination of such low calculated binding energies and high formation energies (see Fig. 6) suggests that $\text{Eu}_{\text{Ga}}\text{-C}_N$ is unlikely to be stable as a complex under thermodynamic equilibrium.

$\text{Eu}_{\text{Ga}}\text{-O}_N$ has one defect level in the bulk band gap: $(+/0)$ is at 1.26 eV (1.23 eV) below the CBM for the basal (axial) geometric configuration. The basal configuration is lower in energy than the axial one (not included in Fig. 6) by 0.18 eV (0.15 eV) when in its 0 (+) charge state. $(\text{Eu}_{\text{Ga}}\text{-O}_N)^0$ is a complex of Eu_{Ga}^0 and O_N^+ , whereas $(\text{Eu}_{\text{Ga}}\text{-O}_N)^+$ is a complex of Eu_{Ga}^+ and O_N^+ . In the basal configuration, the Eu-O distance is 2.29 Å (2.23 Å) in the 0 (+) charge state; see Fig. 7(c). $\text{Eu}_{\text{Ga}}\text{-O}_N$ can have a much lower formation energy than the unassociated

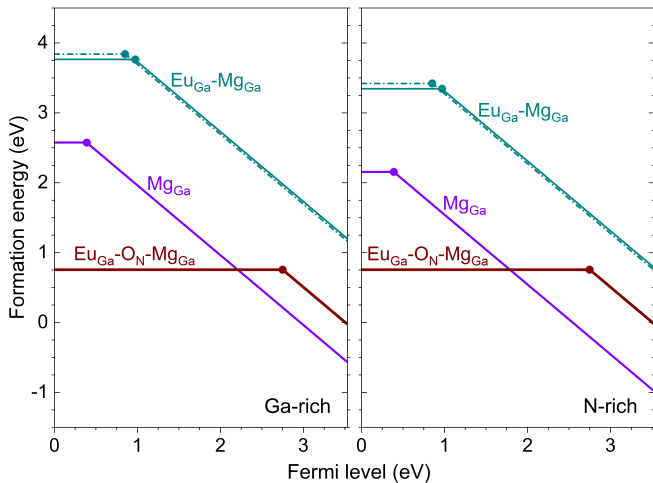


FIG. 8. Formation energies of Mg_{Ga} and related defect complexes $\text{Eu}_{\text{Ga}}\text{-Mg}_{\text{Ga}}$ and $\text{Eu}_{\text{Ga}}\text{-O}_{\text{N}}\text{-Mg}_{\text{Ga}}$ in GaN, plotted as a function of Fermi level from the VBM to the CBM, under the Ga-rich and N-rich conditions. For each defect, only segments corresponding to the lowest-energy charge states are shown. Large solid dots connecting two segments with different slopes mark the defect levels. Two $\text{Eu}_{\text{Ga}}\text{-Mg}_{\text{Ga}}$ configurations, corresponding to the structures in Fig. 9(a) and 9(b), are reported.

Eu_{Ga} , as seen in Fig. 6. Similarly, $\text{Eu}_{\text{Ga}}\text{-Si}_{\text{Ga}}$ introduces the (+/0) level at 1.04 eV below the CBM. $(\text{Eu}_{\text{Ga}}\text{-Si}_{\text{Ga}})^0$ is a complex of Eu_{Ga}^- and Si_{Ga}^+ , whereas $(\text{Eu}_{\text{Ga}}\text{-Si}_{\text{N}})^+$ is a complex of Eu_{Ga}^0 and Si_{Ga}^+ . The Eu–Si distance is 3.25 Å (3.27 Å) in the 0 (+) charge state; see Fig. 7(d).

The electronic behavior of $\text{Eu}_{\text{Ga}}\text{-C}_{\text{N}}$ is thus similar to that of $\text{Er}_{\text{Ga}}\text{-C}_{\text{N}}$ [57]. Other defect complexes are different. For example, $\text{Er}_{\text{Ga}}\text{-O}_{\text{N}}$ is a shallow donor and thus has no defect levels in the bulk band gap; $\text{Er}_{\text{Ga}}\text{-H}_i$ introduces the (+/–) level [57] instead of (+/0) like in the case of $\text{Eu}_{\text{Ga}}\text{-H}_i$. This, again, illustrates the difference between Er and the mixed-valence Eu in GaN.

D. Defect complexes of Eu, O, and Mg

We now focus on possible interaction between Eu, Mg, and O in GaN. Figure 8 shows the calculated formation energy of Mg-related defects. The unassociated Mg_{Ga} has the (0/–) level at 0.39 eV above the VBM, in reasonable agreement with previous studies [64, 65]. It is noted that “ Mg_{Ga}^0 ” is not a true charge state of Mg_{Ga} , but a defect complex consisting of Mg_{Ga}^- and an electron hole (h^*) localized on one of the basal N atoms. The Mg–N distance is 2.22 Å for the N atom that hosts h^* and 2.00–2.01 Å for the other N atoms. The axial configuration of Mg_{Ga}^0 is 10 meV higher in energy than the basal one. A metastable configuration of Mg_{Ga}^0 in which the hole is delocalized over *all* N atoms is 0.19 eV higher in energy than the ground-state one. In this configuration, all the Mg–N distances are almost equal (2.02–2.04 Å).

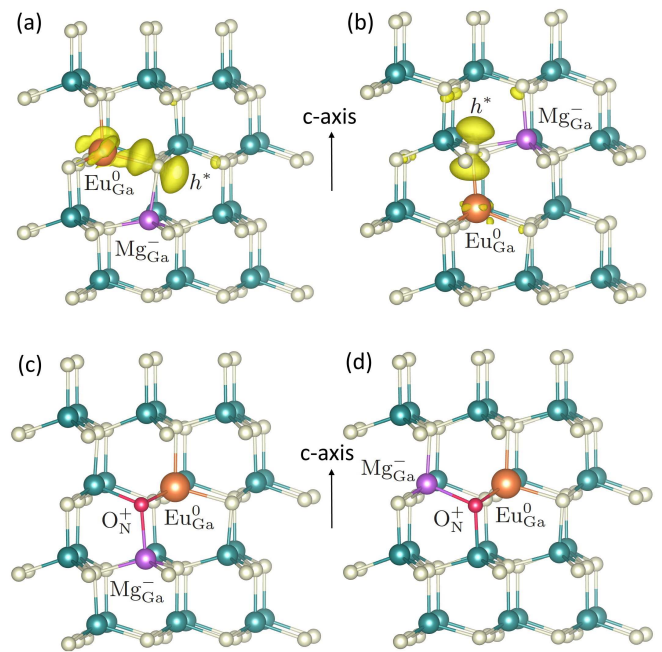


FIG. 9. Structure of Mg-related defect complexes: $(\text{Eu}_{\text{Ga}}\text{-Mg}_{\text{Ga}})^0$ [(a) and (b)] and $(\text{Eu}_{\text{Ga}}\text{-O}_{\text{N}}\text{-Mg}_{\text{Ga}})^0$ [(c) and (d)]. Large spheres are Eu, medium Ga/Mg, and small N/O. Charge densities associated with the localized hole h^* in the $(\text{Eu}_{\text{Ga}}\text{-Mg}_{\text{Ga}})^0$ configuration are visualized as (yellow) isosurfaces; the isovalue for the isosurface is set to $0.05 e/\text{Å}^3$.

$\text{Eu}_{\text{Ga}}\text{-Mg}_{\text{Ga}}$ has a defect level, (0/–), at 0.97 eV or 0.85 eV above the VBM, see Fig. 8, depending on specific geometric configurations. $(\text{Eu}_{\text{Ga}}\text{-Mg}_{\text{Ga}})^0$ is a complex consisting of Eu_{Ga}^0 , Mg_{Ga}^- , and h^* , whereas $(\text{Eu}_{\text{Ga}}\text{-Mg}_{\text{Ga}})^-$ is a complex of Eu_{Ga}^0 and Mg_{Ga}^- . Figure 9(a) shows the lowest-energy configuration of $(\text{Eu}_{\text{Ga}}\text{-Mg}_{\text{Ga}})^0$ in which h^* resides on the N atom that is basally (axially) bonded to Eu (Mg). Other configurations, such as that shown in Fig. 9(b), are 38–75 meV higher in energy. In the basal (with respect to Eu) configuration, see Figure 9(a), the distance between Mg and the N site that bridges Mg and Eu is 2.12 Å (2.02 Å) when the complex is in the 0 (–) charge state. The presence of h^* on that N atom thus slightly elongates the Mg–N bond. The Eu–N distance is also longer for the N atom that hosts h^* [2.23 Å, compared to 2.25 Å (2.18 Å) for the axial (other basal) Eu–N bonds in $(\text{Eu}_{\text{Ga}}\text{-Mg}_{\text{Ga}})^0$]. In the axial configuration, see Figure 9(b), the distance between Mg and the N site that bridges Mg and Eu is also longer when h^* is on that N atom: the Mg–N bond length is 2.09 Å (2.01 Å) in $(\text{Eu}_{\text{Ga}}\text{-Mg}_{\text{Ga}})^{0(-)}$. The calculated binding energy of $(\text{Eu}_{\text{Ga}}\text{-Mg}_{\text{Ga}})^-$ is almost zero, suggesting that $\text{Eu}_{\text{Ga}}\text{-Mg}_{\text{Ga}}$ may be not stable as a complex when incorporated under n-type, thermodynamic equilibrium growth conditions (see also discussion in Sec. IV A).

Note that, unlike Mg_{Ga}^0 , a metastable state of $(\text{Eu}_{\text{Ga}}\text{-Mg}_{\text{Ga}})^0$ in which the hole is delocalized over the N atoms cannot be stabilized (even at the DFT-GGA [66] level of

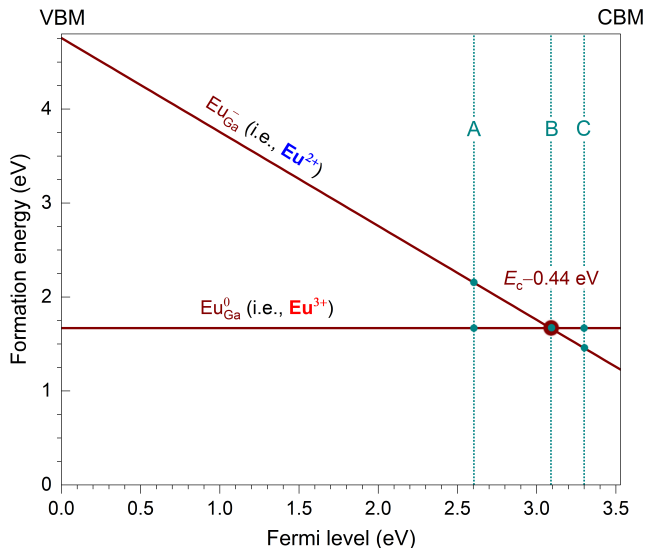


FIG. 10. The formation energy of the negatively charged configuration of Eu_{Ga} is dependent on the Fermi-level position. This allows for the tuning of the $\text{Eu}^{2+}/\text{Eu}^{3+}$ ratio by shifting the Fermi level, e.g., through co-doping; see the text.

the calculations where the electronic states tend to be over-delocalized). This is due to the local lattice distortion caused by the presence of Eu in the complex.

Finally, we consider a complex consisting of Eu_{Ga} , O_{N} , and Mg_{Ga} . $\text{Eu}_{\text{Ga}}\text{-O}_{\text{N}}\text{-Mg}_{\text{Ga}}$ introduces one defect level in the band gap: $(0/-)$ at 0.78 eV below the CBM; see Fig. 8. The neutral charge state, $(\text{Eu}_{\text{Ga}}\text{-O}_{\text{N}}\text{-Mg}_{\text{Ga}})^0$, is a defect complex consisting of Eu_{Ga}^0 , O_{N}^+ , and Mg_{Ga}^- , whereas $(\text{Eu}_{\text{Ga}}\text{-O}_{\text{N}}\text{-Mg}_{\text{Ga}})^-$ is a complex of Eu_{Ga}^- , O_{N}^+ , and Mg_{Ga}^- ; see also Table I. Figures 9(c) and 9(d) show the two lowest configurations of the neutral charge state which have almost equal energies with the former 10 meV lower in energy than the latter. Both charge states can have significantly lower formation energies than those of the other defects and relatively high binding energies.

IV. DISCUSSION

A. Tuning the Eu valence and concentration through co-doping and defect association

Our results clearly show that Eu can be stable as Eu^{2+} and/or Eu^{3+} in GaN. Figure 10 highlights the dependence of the $\text{Eu}^{2+}/\text{Eu}^{3+}$ ratio on the position of Fermi level (μ_e). For $\mu_e < E_c - 0.44$ eV, the formation energy of Eu_{Ga}^0 is lower than that of Eu_{Ga}^- . At position A, for example, the concentration of Eu_{Ga}^0 is much larger than that of Eu_{Ga}^- and hence $c(\text{Eu}^{2+})/c(\text{Eu}^{3+}) \ll 1$. At $\mu_e = E_c - 0.44$ eV (i.e., position B), Eu_{Ga}^0 and Eu_{Ga}^- have equal concentrations; i.e., $c(\text{Eu}^{2+})/c(\text{Eu}^{3+}) = 1$. For $\mu_e > E_c - 0.44$ eV, Eu_{Ga}^- is energetically more stable than

Eu_{Ga}^0 ; at position C, e.g., $c(\text{Eu}^{2+})/c(\text{Eu}^{3+}) \gg 1$. Even a small shift in the Fermi-level position (hence a small change in the formation energy of Eu_{Ga}^-) can lead to a large change in the Eu^{2+} concentration; see Eq. (2).

As shallow donors, O and Si can make GaN n-type or, at least, shift the Fermi level toward the CBM as the charge neutrality condition [Eq. (3)] is re-established. When the Fermi level moves closer to the CBM, the n-type carrier concentration increases. In the case of Eu-doped GaN, O and/or Si co-doping can be employed to control the charge state of Eu_{Ga} and thus the valence state of Eu. For example, with an appropriate concentration of the co-dopants, the Fermi level of the material can be “pinned” near or above $E_c - 0.44$ eV where the concentration of Eu^{2+} is high (See below for a discussion of relevant reported experiments). Donor-like defects such as the positively charged configurations of V_{N} and H_i can have similar effects, although they are expected to be much less effective than the shallow donors in shifting the Fermi level. We emphasize that these are *global* effects since those defects do not need to be close to Eu_{Ga} for the Fermi-level shift to happen; the defect-defect interaction takes place only indirectly via the interaction with the common electron reservoir [i.e., μ_e in Eq. (1)].

The effects of defect association and thus *local* defect-defect interaction are investigated by considering defect complexes explicitly, as presented in Sec. III. Overall, we find that the electronic behavior of complexes is significantly different from that of their unassociated constituents. Defect levels associated with the complexes are shifted, compared to those associated with the isolated ones, and additional levels may form as a result of strong local elastic and electrostatic interactions between constituents in the complexes. Notably, the valence state of Eu can be controlled through defect association. For example, Eu^{2+} is found to be more stable in complexes with V_{N} , H_i , O_{N} , and Si_{Ga} , compared to that in the unassociated Eu_{Ga} . This is mainly due to the strong Coulomb attraction between Eu_{Ga}^- and the positively charged native defect in the neutral complex configuration (See a detailed discussion in the case of $\text{Eu}_{\text{Ga}}\text{-}V_{\text{N}}$ in Sec. III B). In complexes with C_{N} and Mg_{Ga} , Eu is stable only as Eu^{3+} , largely determined by the available stable charge states of C_{N} and Mg_{Ga} . Defect association also changes the formation energy and can thus affect defect incorporation during growth. Complexes of Eu_{Ga} and O_{N} can have a much lower formation energy than the unassociated Eu_{Ga} , indicating that co-doping with O makes it easier to incorporate Eu into GaN. The formation energy is significantly lower in the case of $\text{Eu}_{\text{Ga}}\text{-O}_{\text{N}}\text{-Mg}_{\text{Ga}}$.

The results summarized in Table I also show that the binding energy varies significantly from one defect complex to another. Having a positive calculated binding energy, however, does not mean that the defect complex will readily form. As discussed in Ref. [49], under thermodynamic equilibrium, the binding energy needs to be greater than the larger of the formation energies of the isolated constituent defects for the complex to have

higher concentration than its constituents. On the other hand, a small calculated binding energy does not necessarily mean that the complex cannot occur with a significant concentration since it can still form under non-equilibrium growth conditions and get trapped inside the material. (Eu,Mg)-doped GaN, for example, has often been made by ion-implanting with Eu fluences [30, 31] or prepared by molecular-beam epitaxy (MBE) [26, 27]. Defect complexes such as $\text{Eu}_{\text{Ga}}\text{-Mg}_{\text{Ga}}$ thus can still exist despite having a very small binding energy. Overall, one should expect that defects are present in the material in both the unassociated and associated forms.

Our results for the unassociated Eu_{Ga} showing Eu^{2+} more stable than Eu^{3+} only in a small range of Fermi-level values near the CBM, see Fig. 2 or 10, thus explain why Eu^{3+} is often found to be predominant in Eu-doped GaN samples. Experimentally, a significant Eu^{2+} concentration occurs only when prepared under certain conditions [19, 20]. Mitchell et al. [19] were able to achieve $c(\text{Eu}^{2+})/c(\text{Eu}^{3+}) > 1$ when using both O and Si as co-dopants and suitable growth conditions. Nunokawa et al. [20] reported similar achievement with their (Eu,Si,O)-doped GaN. Notably, all their samples exhibited n-type conductivity [20], which is consistent with our results showing the $\epsilon(0/-)$ level of Eu_{Ga} , i.e., the $\text{Eu}^{3+/2+}$ level, close to the CBM. A measurement of the Fermi level as a function of the O and Si concentration should be able to confirm our prediction of this defect level. Note that the Eu-doped GaN/SiO₂ nanocomposites reported in Ref. [18] can be regarded as Eu-doped GaN being co-doped with O and Si, and Eu^{2+} is expected to be present predominantly at/near the interface.

The relatively low temperature (e.g., 700°C instead of 1030°C) used during growth via OMVPE also appeared to play a key role in increasing the Eu^{2+} concentration [19, 20, 22]. This is likely because decreasing the temperature leads to an increase in the concentration of complexes and a decrease in the concentration of their isolated constituents; see a discussion in Ref. [49]. In other words, it is easier to incorporate Eu into GaN in the form of complexes such as the low-formation-energy $\text{Eu}_{\text{Ga}}\text{-O}_{\text{N}}$ at lower growth temperatures. The temperature, of course, cannot be too low as the concentration of thermally activated defects is still governed by Eq. (2).

B. Eu-related defects as carrier traps for Eu^{3+} intra-*f* luminescence

We now focus on the electronic behavior of the Eu-related defects and discuss their possible role in intra-*f* luminescence through non-resonant excitation of the Eu^{3+} ion; see Fig. 1. As reported earlier, the unassociated Eu_{Ga} has defect levels in the host band gap. The $(0/-)$ level can act as an electron trap. The electron-capturing defect configuration is Eu_{Ga}^0 , which is essentially Eu^{3+} . When Eu_{Ga}^0 captures an electron from the conduction band (e.g., previously excited from the va-

lence band to the conduction band under band-to-band excitation) and becomes Eu_{Ga}^- (assuming that the system has enough time to relax to its equilibrium configuration), the valence state of Eu changes from trivalent to divalent. The captured electron in Eu_{Ga}^- then recombines non-radiatively with a free hole from the valence band or a hole at some acceptor level and transfer the recombination energy into the Eu^{3+} 4*f*-core. The $(+/0)$ level can act as a hole trap. Compared to Eu-related complexes discussed below, the unassociated Eu_{Ga} traps are expected to be less effective since there is no Coulomb attraction between the carrier and the carrier-capturing configuration (Eu_{Ga}^0). Note that the carrier capture cross section can decrease by orders of magnitude in going from Coulomb attractive defect centers (e.g., $\sim 10^{-12}\text{-}10^{-15}$ cm²) to neutral centers ($\sim 10^{-15}\text{-}10^{-17}$ cm²) to repulsive centers ($\sim 10^{-22}$ cm²) [67]. The relatively small energy separation between the defect level and the band edge may also increase the likelihood of the captured carrier being thermally re-excited into the band.

Experimentally, the unassociated Eu_{Ga} is believed by many to be the dominant Eu^{3+} center in Eu-doped GaN samples [5, 7, 8]. The luminescence center is often characterized by its high relative abundance (up to more than 97% of the incorporated Eu) [9, 10], low-efficiency energy transfer from the GaN host into the Eu^{3+} 4*f*-core (the effective excitation cross section $\sim 1.2 \times 10^{-17}$ cm²) [9, 10, 12], and strong thermal quenching [12]. These descriptions appear to be consistent with the characteristics of the unassociated Eu_{Ga} center reported in this work.

For $\text{Eu}_{\text{Ga}}\text{-V}_{\text{N}}$, the $(+/0)$ level can act as a deep electron trap. An electron is likely to be captured at the V_{N}^+ part of the carrier-capturing defect configuration ($\text{Eu}_{\text{Ga}}\text{-V}_{\text{N}}^+$), due to the Coulomb attraction. This trap is 1.86 eV above the VBM, slightly smaller than the separation (2.12 eV) [4] between the 7F_0 and 5D_0 levels of Eu^{3+} . Note, however, that the error bar in our calculation of the defect level is about 0.1 eV; thus the trap may actually be slightly higher and the energy obtained from a non-radiative recombination of the trapped electron at the $(+/0)$ level and a hole may be large enough to excite an electron from 7F_0 to 5D_0 . In other words, we cannot completely rule out the role of $\text{Eu}_{\text{Ga}}\text{-V}_{\text{N}}$ as an electron trap and a defect center for the ${}^5D_J \rightarrow {}^7F_J$ transitions, although it is very likely that the complex has a limited role in high-energy luminescent transitions. The defect levels nearer to the VBM, $(3+/2+)$ and $(2+/+)$, may act as hole traps; however, their hole-capture efficiency should be very low given the Coulomb repulsion between the carrier and the positively charged (V_{N}^{3+} or V_{N}^+) part in the hole-capturing defect configuration of $\text{Eu}_{\text{Ga}}\text{-V}_{\text{N}}$.

For $\text{Eu}_{\text{Ga}}\text{-V}_{\text{Ga}}$, the defect levels nearer to the VBM and CBM may act as hole and electron traps, respectively. However, they are unlikely to be efficient due to the Coulomb repulsion between the carrier and certain parts of the carrier-capturing defect configurations; see Fig. 5. The traps formed by $\text{Eu}_{\text{Ga}}\text{-C}_{\text{N}}$ are also expected not to be very efficient because the carrier-capturing de-

fect configuration $(\text{Eu}_{\text{Ga}}\text{-C}_{\text{N}})^0$ is all neutral; see Fig. 7(b).

The $(+ / 0)$ level of $\text{Eu}_{\text{Ga}}\text{-H}_i$, $\text{Eu}_{\text{Ga}}\text{-O}_{\text{N}}$, and $\text{Eu}_{\text{Ga}}\text{-Si}_{\text{Ga}}$ is expected to be an efficient deep electron trap. An excited electron from the conduction band is likely to be captured at the positively charged $(\text{H}_i^+, \text{O}_{\text{N}}^+, \text{or Si}_{\text{Ga}}^+)$ part of the carrier-capturing defect configuration, due to the Coulomb attraction; see Fig. 7(a), 7(c), and 7(d). In the case of $\text{Eu}_{\text{Ga}}\text{-O}_{\text{N}}$, for example, since the neutral charge state of O_{N} is energetically unstable, the captured electron is likely transferred to the Eu_{Ga}^0 part and transforms it into Eu_{Ga}^- , assuming the system is allowed to relax to its equilibrium configuration, and hence $(\text{Eu}_{\text{Ga}}\text{-O}_{\text{N}})^+$ becomes $(\text{Eu}_{\text{Ga}}\text{-O}_{\text{N}})^0$ which then recombines with a hole and the energy is transferred into the Eu $4f$ -core.

Regarding the Mg-containing defect complexes, the $(0 / -)$ level of $\text{Eu}_{\text{Ga}}\text{-Mg}_{\text{Ga}}$ can act as a deep hole trap. A hole from the valence band (e.g., previously created by exciting an electron from the valence band to the conduction band) can be efficiently captured at the negatively charged $(\text{Mg}_{\text{Ga}}^-)$ part of the carrier-capturing defect configuration $(\text{Eu}_{\text{Ga}}\text{-Mg}_{\text{Ga}})^-$; see Table I. Finally, the $(0 / -)$ level of $\text{Eu}_{\text{Ga}}\text{-O}_{\text{N}}\text{-Mg}_{\text{Ga}}$ can act as an electron trap with the carrier likely being captured at the O_{N}^+ part of $(\text{Eu}_{\text{Ga}}\text{-O}_{\text{N}}\text{-Mg}_{\text{Ga}})^0$. The behavior of this neutral configuration should be similar to that of $(\text{Eu}_{\text{Ga}}\text{-O}_{\text{N}})^+$ described above.

Altogether we find that $\text{Eu}_{\text{Ga}}\text{-O}_{\text{N}}$, $\text{Eu}_{\text{Ga}}\text{-Si}_{\text{Ga}}$, $\text{Eu}_{\text{Ga}}\text{-H}_i$, $\text{Eu}_{\text{Ga}}\text{-Mg}_{\text{Ga}}$, $\text{Eu}_{\text{Ga}}\text{-O}_{\text{N}}\text{-Mg}_{\text{Ga}}$, and possibly $\text{Eu}_{\text{Ga}}\text{-V}_{\text{N}}$ are efficient defect-related Eu^{3+} centers for non-resonant excitation. The significant local distortion around the Eu^{3+} ion should help relax the Laporte selection rules and allows for bright emission. As discussed above, they are efficient carrier traps and thus likely to have high carrier capture cross sections. The energy transfer from the GaN host into the Eu^{3+} $4f$ -core is also expected to be efficient, given the close proximity of the carrier-capturing part to the Eu^{3+} ion in the carrier-capturing defect configuration. Experimentally, it was shown that efficient energy transfer into the Eu $4f$ -core and a high concentration of the Eu-related defect centers is key to enhanced emission intensity [68]. Our findings are thus consistent with experimental observations showing that the Eu^{3+} PL emission was significantly enhanced in GaN co-doped with Eu and O [19, 21, 22], Si [28], or Mg [23–27].

We now comment on the PL hysteresis observed in (Eu,Mg)-doped GaN, believed to involve hysteretic photochromic switching (HPS) between two defect configurations, namely “Eu0” and “Eu1(Mg)”, in which the Eu^{3+} ion experiences slightly different local crystal fields [29–31]. The authors identified “Eu0” and “Eu1(Mg)” with the so-called “shallow transient state” (STS) and “deep ground state” (DGS), respectively, proposed by Lany and Zunger [64] for Mg_{Ga}^0 in Mg-doped GaN. The DGS is equivalent to the Mg_{Ga}^0 configuration consisting of Mg_{Ga}^- and h^* in our work and the STS can be identified with the metastable configuration described in Sec. III D. One assumption made by O’Donnell et al. [30] was that, in (Eu,Mg)-doped GaN, Eu could be regarded as a “spectator ion”. This may not be the case as we find that, e.g.,

the $(0 / -)$ level of $\text{Eu}_{\text{Ga}}\text{-Mg}_{\text{Ga}}$ is shifted by ~ 0.5 eV from that of Mg_{Ga} and the local lattice environment and hence the ability to accommodate a metastable state is different for $(\text{Eu}_{\text{Ga}}\text{-Mg}_{\text{Ga}})^0$ and Mg_{Ga}^0 ; see Sec. III D. Note that Mg in (Eu,Mg)-doped GaN is expected to be present both as the unassociated Mg_{Ga} and in $\text{Eu}_{\text{Ga}}\text{-Mg}_{\text{Ga}}$. And it is not clear at this point if the perturbation is strong enough to cause the observed PL hysteresis when Mg_{Ga} and Eu_{Ga} are far apart such that the metastable configuration of Mg_{Ga}^0 can be stabilized. Besides, we find the total-energy difference between the stable and metastable configurations of Mg_{Ga}^0 is rather large (0.19 eV).

In (Eu,O,Mg)-doped GaN, Cameron et al. [32] observed another Eu^{3+} center denoted as “Eu0(Ox)” in addition to “Eu1(Mg)” and “Eu0”. Eu0(Ox) was found to be stable over a prolonged excitation time and a wide temperature range, unlike the other two Eu^{3+} centers. The center can be identified with the $\text{Eu}_{\text{Ga}}\text{-O}_{\text{N}}\text{-Mg}_{\text{Ga}}$ complex in our calculations which should co-exist with smaller defect complexes such as $\text{Eu}_{\text{Ga}}\text{-Mg}_{\text{Ga}}$ and the unassociated defects. With its low formation energy, the complex is expected to occur with a significant concentration. The main difference between $\text{Eu}_{\text{Ga}}\text{-Mg}_{\text{Ga}}$ and $\text{Eu}_{\text{Ga}}\text{-O}_{\text{N}}\text{-Mg}_{\text{Ga}}$ is that upon capturing a hole the negatively charged state of the former becomes $(\text{Eu}_{\text{Ga}}\text{-Mg}_{\text{Ga}})^0$ with a localized hole residing at the bridging N atom, whereas upon capturing an electron the neutral state of the latter becomes $(\text{Eu}_{\text{Ga}}\text{-O}_{\text{N}}\text{-Mg}_{\text{Ga}})^-$ with the valence change occurring on the Eu ion; all assuming the system is allowed to relax to its equilibrium configuration.

C. Eu-related defects as carrier traps for defect-to-band luminescence

In addition to intra- f luminescence, Eu-related defects can also act as carrier traps in defect-to-band transitions that emit light in the visible range. In n-type GaN, the unassociated Eu_{Ga} is stable as Eu_{Ga}^- . This defect configuration can capture a hole from the VBM (e.g., left by an electron previously excited to from the valence to the conduction band) and emits a photon. The peak emission energy corresponds to the transition level $E_{\text{opt}}^{-/0}$, i.e., the energy difference between Eu_{Ga}^- and Eu_{Ga}^0 in the lattice configuration of Eu_{Ga}^- . As shown in Fig. 11(a), this emission peak is at 2.66 eV, with a relaxation energy of 0.43 eV. Our results thus indicate that Eu_{Ga} is a source of blue luminescence in n-type GaN, which may explain the broad blue emission observed in the Eu^{2+} -containing GaN/SiO₂ nanocomposites [18]. It should be emphasized that the mechanism we present here is different from that associated with the so-called $4f^65d^1 \rightarrow 4f^7$ transition within the Eu^{2+} ion mentioned in Ref. [18] and often regarded in the literature as the cause for blue luminescence observed in Eu^{2+} -containing materials. In p-type GaN, Eu_{Ga} is stable as Eu_{Ga}^+ ; the emission peak corresponds to the $\text{Eu}_{\text{Ga}}^+ \rightarrow \text{Eu}_{\text{Ga}}^0$ transition, after capturing an electron from the CBM, is also 2.66 eV (blue), see Fig. 11(b).

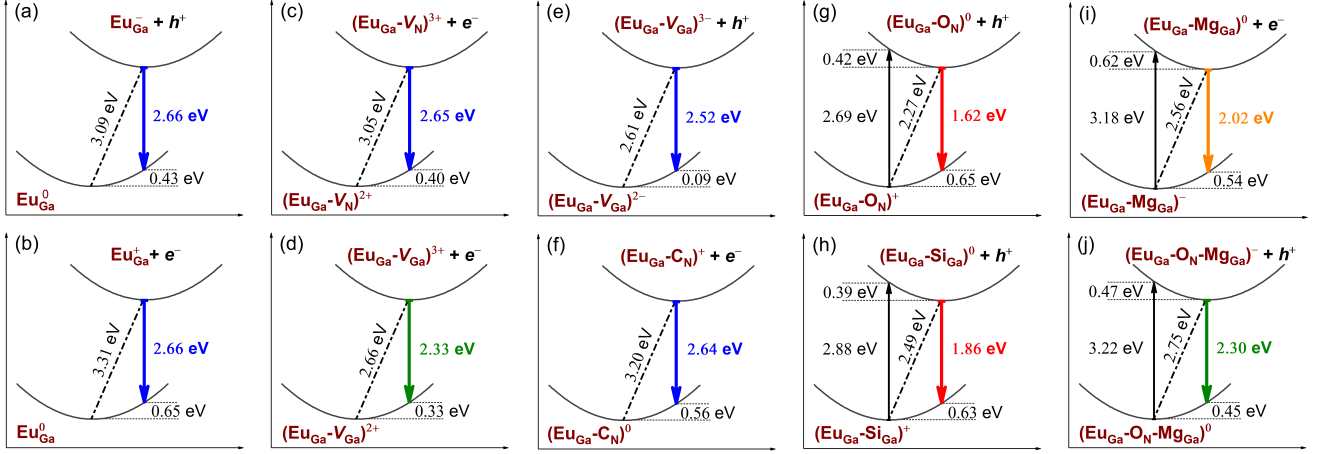


FIG. 11. Configuration-coordinate diagrams illustrating optical emission (down arrow) and absorption (up arrow) processes involving Eu-related defects in GaN. The thermal energy [also called the zero-phonon line (ZPL); the dash-dotted line] is the thermodynamic transition level $\epsilon(q/q')$ relative to the VBM [in the case of hole (h^+) capture] or CBM [electron (e^-) capture]. The values sandwiched between two dotted lines are the relaxation energies (the Franck-Condon shifts). Only transitions with emissions in the visible range and the absorption peaks that fall within the host band gap are included. Axes are not to scale.

Similar calculations are carried out for Eu-related defect complexes, as shown in Figs. 11(c)–11(j). In n-type GaN, for example, $(\text{Eu}_{\text{Ga}}-\text{V}_{\text{Ga}})^{3-}$ can give rise to broad emission peaked at 2.52 eV (blue), $(\text{Eu}_{\text{Ga}}-\text{O}_{\text{N}})^0$ at 1.62 eV (red), $(\text{Eu}_{\text{Ga}}-\text{Si}_{\text{Ga}})^0$ at 1.86 eV (red), and $(\text{Eu}_{\text{Ga}}-\text{O}_{\text{N}}-\text{Mg}_{\text{Ga}})^-$ at 2.30 eV (green), after capturing a hole from the VBM. Each of these defect configurations is the most stable charge state of its respective defect under n-type conditions; see Sec. III. In p-type GaN, $(\text{Eu}_{\text{Ga}}-\text{V}_{\text{N}})^{3+}$ can give rise to broad emission peaked at 2.65 eV (blue), $(\text{Eu}_{\text{Ga}}-\text{V}_{\text{Ga}})^{3+}$ at 2.33 eV (green), $(\text{Eu}_{\text{Ga}}-\text{C}_{\text{N}})^+$ at 2.64 eV (blue), and $(\text{Eu}_{\text{Ga}}-\text{Mg}_{\text{Ga}})^0$ at 2.02 eV (orange), after capturing an electron from the CBM. Each of these defect configurations is the most stable charge state of its respective defect under p-type conditions. We also consider the absorption process. In the case of $\text{Eu}_{\text{Ga}}-\text{Mg}_{\text{Ga}}$, for example, an electron can be excited from $(\text{Eu}_{\text{Ga}}-\text{Mg}_{\text{Ga}})^-$ to the conduction band, with a peak absorption energy of 3.18 eV, given by the energy difference between $(\text{Eu}_{\text{Ga}}-\text{Mg}_{\text{Ga}})^-$ and $(\text{Eu}_{\text{Ga}}-\text{Mg}_{\text{Ga}})^0$, both in the lattice configuration of the negatively charged configuration.

The above-mentioned Eu-related defects can thus be sources of broad blue, green, red, and orange defect-to-band luminescence in n- or p-type GaN samples.

V. CONCLUSIONS

We have carried out a systematic study of defects in Eu-doped GaN using hybrid density-functional calculations. The material is found to exhibit rich defect physics resulting from the ability of Eu to be mixed-valence and the interaction between the RE dopant and native defects and (intentional or otherwise) impurities. Eu can be stable as divalent and/or trivalent when incorporated

at the Ga site in GaN, and the $\text{Eu}^{2+}/\text{Eu}^{3+}$ ratio is dependent on the position of Fermi level and thus the growth conditions. We have discussed the tuning of the Eu valence state and concentration in terms of *global* and *local* effects caused by indirect and direct defect-defect interactions through co-doping and defect association, respectively. Based on a detailed analysis of the defects' local lattice environment and electronic behavior, the unassociated Eu_{Ga} is identified as an optically active center for sharp red Eu^{3+} intra- f luminescence. Eu-related defect complexes such as $\text{Eu}_{\text{Ga}}-\text{O}_{\text{N}}$, $\text{Eu}_{\text{Ga}}-\text{Si}_{\text{Ga}}$, $\text{Eu}_{\text{Ga}}-\text{H}_i$, $\text{Eu}_{\text{Ga}}-\text{Mg}_{\text{Ga}}$, and $\text{Eu}_{\text{Ga}}-\text{O}_{\text{N}}-\text{Mg}_{\text{Ga}}$ are expected to be more efficient for non-resonant excitation of Eu^{3+} , whereas $\text{Eu}_{\text{Ga}}-\text{V}_{\text{Ga}}$ is unlikely to be efficient. $\text{Eu}_{\text{Ga}}-\text{V}_{\text{N}}$ is likely to have a limited role in intra- f high-energy luminescence. Eu-related defects can also act as carrier traps for defect-to-band transitions that emit visible light. The unassociated Eu_{Ga} , for example, can be a source of the broad blue emission observed in n-type, Eu^{2+} -containing GaN.

ACKNOWLEDGMENTS

This work made use of resources in the Center for Computationally Assisted Science and Technology (CCAST) at North Dakota State University.

Appendix A: Effects of the semicore Ga 3d electrons

Figure 12 shows the total and Ga 3d-projected electronic densities of states (DOS) of bulk GaN in calculations using the Heyd-Scuseria-Ernzerhof (HSE) functional [47], in which the semicore Ga 3d electrons are either (a) treated as core states or (b) explicitly included in

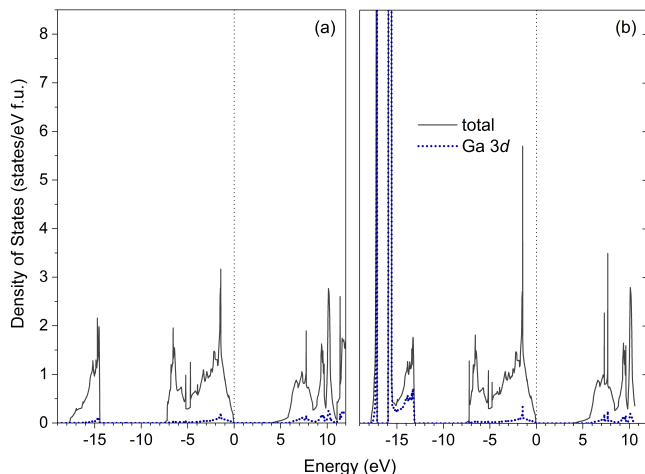


FIG. 12. Total and projected densities of states of bulk GaN obtained in calculations where the Ga 3d electrons are (a) treated as core states or (b) explicitly included in the valence. The zero of energy is set to the highest occupied state.

the valence. The Ga 3d states are found to be deep in the valence band (>15 eV below the VBM). The inclusion of the Ga 3d electrons as valence electrons slightly changes the lattice parameters and band gap value. To match the experimental band gap, we set the Hartree-Fock mixing parameter (α) to 0.310 in the Ga 3d-as-core calculation and 0.295 in the Ga 3d-as-valence calculation. The former gives $a = 3.1964$ Å and $c = 5.1883$ Å; the latter gives $a = 3.1819$ Å and $c = 5.1693$ Å; here, the atomic structure of GaN in the two cases is fully optimized within the HSE functional with the respective α values.

Our tests for Eu_{Ga} show that its $\epsilon(0/-)$ level is 0.55 eV below the CBM in the Ga 3d-as-valence HSE calculations, which is 0.11 eV greater than that obtained in the Ga 3d-as-core calculations. The difference is within the typical error bar in our calculations (expected to be about 0.1 eV for singly charged defects). The effects of the semicore electrons thus do not affect the physics of what we are presenting and our conclusions. Note that the inclusion of the Ga 3d electrons in the valence (which results in a 125% increase in the total number of valence electrons in the supercell) is computationally much more demanding, making it prohibitive to carry out calculations for a large number of defect configurations.

Appendix B: Electronic structure of Eu- versus Er-doped GaN

Figure 13 show the total and Eu 4f-projected electronic densities of states of Eu-doped GaN obtained in DFT+ U [69] and HSE [47]. In both methods, the DFT part is based on the Perdew-Burke-Ernzerhof (PBE) parametrization [66] of the generalized gradient approximation (GGA). In these calculations, one Ga atom in the 96-atom GaN supercell is substituted with europium

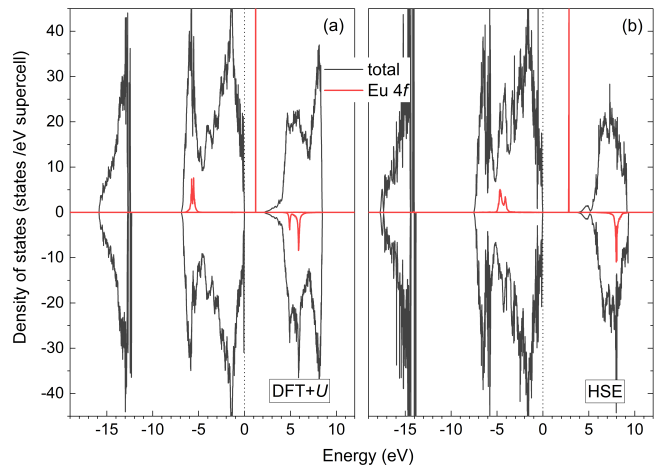


FIG. 13. Total and projected densities of states of Eu-doped GaN obtained in calculations using (a) the DFT+ U method ($U^{\text{eff}} = 7$ eV for Eu 4f electrons) or (b) the HSE functional. The zero of energy is set to the highest occupied state.

(Eu); i.e., the chemical composition is $\text{EuGa}_{47}\text{N}_{48}$ (i.e., the Eu concentration $\sim 2\%$), which corresponds to the Eu_{Ga}^0 defect configuration (i.e., Eu^{3+} at the Ga^{3+} lattice site) discussed in the main text. The ground state of Eu^{3+} is $4f^6$. In the calculated DOS, we find that Eu has 6 spin-up occupied 4f states in the valence band, 1 spin-up unoccupied 4f state in the host band gap, and 7 spin-down unoccupied 4f states in the conduction band; see Fig. 13. The presence of the Eu 4f state in the band gap is key to the stability of Eu^{2+} in Eu-doped GaN. An electron when added to the system will occupy the lowest unoccupied state, which is, in this case, the unoccupied in-gap Eu 4f state. Upon capturing the electron, Eu^{3+} ($4f^6$) becomes Eu^{2+} ($4f^7$); or, in our defect notation, Eu_{Ga}^0 becomes Eu_{Ga}^- . The main differences between the DFT+ U and HSE results are (i) in the calculated value of the host band gap and thus the position of the in-gap Eu 4f state with respect to the band edges, and (ii) the position of the Eu 4f levels in the valence and conduction bands.

For comparison, we also perform similar calculations for erbium (Er) doped GaN. Figure 14 show the total and Er 4f-projected electronic densities of states of Er-doped GaN obtained in DFT+ U and HSE calculations. In these calculations, the chemical composition is $\text{ErGa}_{47}\text{N}_{48}$, which corresponds to the Er_{Ga}^0 defect configuration (i.e., Er^{3+} at the Ga^{3+} site) reported in Ref. [57]. The ground state of Er^{3+} is $4f^{11}$. In the calculated DOS, Er has 7 spin-up and 4 spin-down occupied 4f states in the valence band and 3 spin-down unoccupied 4f states in the conduction band. There are no Er 4f states in the band gap or at the band edges of the GaN host. As a result, Er is stable only as Er^{3+} and the unassociated Er_{Ga} is electrically inert as reported in our previous work [57].

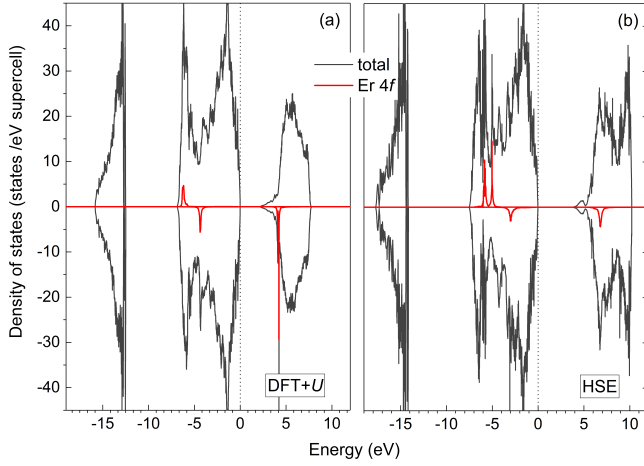


FIG. 14. Total and projected DOS of Er-doped GaN obtained in calculations using (a) the DFT+ U method ($U^{\text{eff}} = U - J = 8$ eV for Er 4 f electrons) or (b) the HSE functional. The zero of energy is set to the highest occupied state.

Appendix C: Charge density associated with Eu_{Ga}^-

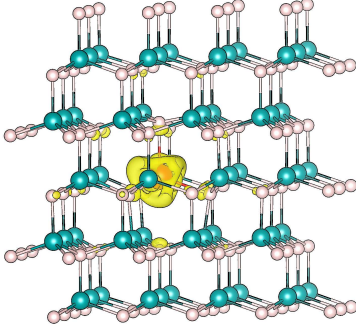


FIG. 15. Structure and charge density associated with Eu_{Ga}^- in GaN. The isovalue for the charge-density isosurface (yellow) is set to $0.02 \text{ e}/\text{\AA}^3$. The large (red) sphere is Eu, medium (blue) spheres are Ga, and small (red) spheres are N.

Figure 15 shows the charge density associated with the extra electron in Eu_{Ga}^- , compared to the neutral defect Eu_{Ga}^0 but in the Eu_{Ga}^- atomic configuration. The electron is highly localized at the Eu site. An examination of the orbital-projected wavefunctions show that the extra electron occupies the previously unoccupied Eu 4 f state in the band gap (see Fig. 13). Thus, upon capturing the electron, the defect configuration Eu_{Ga}^0 (i.e., Eu^{3+}) becomes Eu_{Ga}^0 (Eu^{2+}), as discussed in the main text.

Appendix D: Structure of $(\text{Eu}_{\text{Ga}}-\text{V}_{\text{N}})^{2+}$: basal versus axial

Figure 16 shows the structure of $(\text{Eu}_{\text{Ga}}-\text{V}_{\text{N}})^{2+}$. In the basal geometric configuration, Eu is found to be stable as

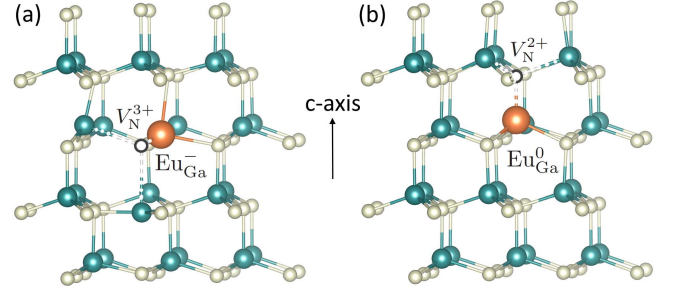


FIG. 16. Structure of $(\text{Eu}_{\text{Ga}}-\text{V}_{\text{N}})^{2+}$: (a) basal and (b) axial geometric configurations. Large spheres are Eu, medium Ga, small N. The nitrogen vacancy is represented by a black circle.

Eu^{2+} , and $(\text{Eu}_{\text{Ga}}-\text{V}_{\text{N}})^{2+}$ a complex of Eu_{Ga}^- and V_{N}^{3+} ; the Eu^{2+} is off-center by 0.58 \AA . This defect configuration is 83 meV lower in energy than another basal configuration where Eu is stable as Eu^{3+} and $(\text{Eu}_{\text{Ga}}-\text{V}_{\text{N}})^{2+}$ is a complex of Eu_{Ga}^0 and V_{N}^{2+} . In the axial geometric configuration, Eu is stable as Eu^{3+} , and $(\text{Eu}_{\text{Ga}}-\text{V}_{\text{N}})^{2+}$ is a complex of Eu_{Ga}^0 and V_{N}^{2+} ; the Eu^{3+} is off-center by only 0.23 \AA . Here, Eu cannot be stabilized as Eu^{2+} in the axial configuration. The difference between the two geometric configurations of $(\text{Eu}_{\text{Ga}}-\text{V}_{\text{N}})^{2+}$ can be understood in terms of their local lattice environment. In this case, it is energetically less unfavorable for the basal configuration to accommodate the larger Eu^{2+} ion by moving the ion significantly off-center. The strong Coulomb interaction between Eu_{Ga}^- and V_{N}^{3+} helps significantly lower the formation energy of that particular defect complex configuration, making it energetically more favorable than the alternative configuration involving Eu^{3+} . Also note that, in the unassociated V_{N} , V_{N}^{2+} is energetically less stable than either V_{N}^+ or V_{N}^{3+} in the entire range of the Fermi-level values from the VBM to the CBM [57, 70, 71].

Appendix E: Comparison with previous calculations

In response to the reviewers' request, we provide in the following a brief summary of relevant computational studies of Eu-doped GaN previously reported in the literature and a comparison with our current work.

Filhol et al. [33] investigated rare-earth (RE) dopants in wurtzite GaN based on DFT within the spin-polarized local-density approximation (LDA). In their calculations, the 4 f electrons of the RE (including Eu) were treated as core states; i.e., Eu, for example, was *a priori assumed* to be Eu^{3+} . Such a computational approach is clearly not suitable for the study of Eu-doped GaN since, as discussed in our work, Eu does introduce a 4 f state in the band gap of the GaN host, and such an electronic state plays an important role in defect formation in the material. The defect energy levels for RE_{Ga} , $\text{RE}_{\text{Ga}}-\text{V}_{\text{N}}$, and $\text{RE}_{\text{Ga}}-\text{V}_{\text{Ga}}$, and $\text{RE}_{\text{Ga}}-\text{O}_{\text{N}}$ reported by Filhol et al., obtained by examining the Kohn-Sham levels at the Γ point, are *qualitatively* different from our results. For

example, Eu_{Ga} and $\text{Eu}_{\text{Ga}}\text{-O}_{\text{N}}$ were reported to be electrically inert and have no defect energy levels in the host band gap [33], which is in contrast to our findings.

Svane et al. [34] studied RE impurities in GaN (and GaAs) using self-interaction corrected, spin-polarized LDA calculations. They found that Eu introduces impurity states in the host band gap; see Fig. 4 of Ref. [34]. As far as the in-gap Eu $4f$ state is concerned, that result is similar to what we observe in Fig. 13. The features involved the Eu $4f$ states in the valence and conduction bands are, however, significantly different from our work [even from our results obtained in DFT+ U calculations; see Fig. 13(a)], which can be ascribed to the different computational methods used. Most importantly, they found that the $\text{Eu}_{\text{Ga}}^{0/-}$ (i.e., $\text{Eu}^{3+/2+}$) level is above the calculated CBM (i.e., Eu is thus stable only as Eu^{3+} in the entire range of the Fermi-level values from the VBM to the CBM), which is *in contrast* to what we find and to the fact that Eu is known to be mixed valence. Note that, in their defect calculations, finite-supercell-size effects were not corrected and the atomic structures were not optimized. Also note that Svane et al. considered zincblende GaN, although both the zincblende and wurtzite structures are expected to show very similar defect physics.

Sanna et al. [35] adopted the LDA+ U scheme within the density-functional-based tight-binding (DFTB) method for their study of RE impurities in wurtzite GaN. The effective U value, U^{eff} , was chosen to be 6.8 eV for the Eu $4f$ states. They found the $\text{Eu}_{\text{Ga}}^{0/-}$ level to be at 1.58 eV above the VBM, much lower than our result ($E_v + 3.09$ eV). Note that the authors did not discuss the stability of Eu^{2+} . If we assume that their Eu_{Ga}^- corresponds to Eu^{2+} , then the result means that Eu^{2+} is stable in a large range of Fermi-level values below the CBM [even larger than the Fermi-level range where Eu^{3+} , i.e., Eu_{Ga}^0 , is more stable]. Such a result is not consistent with what is known experimentally according to which the $\text{Eu}^{2+}/\text{Eu}^{3+}$ ratio is low even under n-type conditions, except when Eu-doped GaN is co-doped with both O and Si [20].

The $\text{Eu}_{\text{Ga}}\text{-V}_{\text{N}}$ complex were reported to have the (+/0) level at 0.27 eV and the (0/-) at 3.14 eV above the VBM; and $\text{Eu}_{\text{Ga}}\text{-V}_{\text{Ga}}$ to have the (0/-) level at 0.5 eV, the (-/2-) level at 0.7 eV, the (2-/3-) level at 1.1 eV, and the (3-/4-) level at 2.59 eV above VBM [35]. These results are *qualitatively* different from those reported in our work. For example, Sanna et al. did not find the (3+/2+) and (2+/+) levels of $\text{Eu}_{\text{Ga}}\text{-V}_{\text{N}}$. These defect levels should be expected to be stable given that V_{N} is stable predominantly in positively charged states in GaN. Note that even for the isolated V_{N} , the most well studied native point defect in GaN, their results (see Fig. 5 of Ref. [35]) were also very different from those obtained in calculations using more advanced methods [57, 70, 71]. The discrepancy can be ascribed mainly to the use of DFTB in the previous work which apparently was not

able to provide an accurate description of defect physics in GaN.

Ouma et al. [36] investigated the $\text{Eu}_{\text{Ga}}\text{-V}_{\text{N}}$ complex in wurtzite GaN using DFT calculations within the generalized gradient approximation (GGA). In their defect calculations, Eu was *assumed* to be stable as Eu^{3+} and finite-size corrections were not included. Their results for the defect complex, with the presence of the (-/2-) and (0/2-) levels, are *qualitatively* different from ours, and not consistent with the fact that V_{N} is stable predominantly in positively charged states. There was no discussion of the stability of the Eu^{2+} ion.

Mitchell et al. [37] reported preliminary results on the local lattice structure and charge density of different charge states of $\text{Eu}_{\text{Ga}}\text{-V}_{\text{Ga}}$, obtained from GGA+ U calculations ($U^{\text{eff}} = 6.8$ eV for Eu $4f$ states). The authors *a priori assumed* the defect complex to have charge states from 0 to 3- and Eu to remain in the trivalent state.

There are studies of Eu-doped GaN that were based on an examination of the electronic density of states obtained in standard DFT (within LDA or GGA) and/or DFT+ U calculations. Goumri-Said et al. [38] in LDA+ U calculations (with $U^{\text{eff}} = 5$ eV for the Eu $4f$ states), for example, found that there were no Eu $4f$ states in the band gap of the zincblende GaN host but $4f$ states in the valence and conduction bands and near the VBM and CBM, respectively; see Fig. 2 of Ref. [38]. Su et al. [39], in GGA+ U ($U^{\text{eff}} = 7.4$ eV) calculations for Eu_{Ga}^0 , also did not find in-gap Eu $4f$ states. Cruz et al. [40], based on their GGA and GGA+ U ($U^{\text{eff}} = 6$ eV) calculations for Eu_{Ga}^0 in wurtzite GaN, also reported similar results. All these results are thus *in contrast* to our finding reported in Fig. 13 and also discussed in the main text. Note that our results obtained in DFT+ U calculations with $U^{\text{eff}} = 5$ eV or 6 eV are very similar to that reported in Fig. 13(a) in which Eu introduces an in-gap $4f$ state. This may suggest that, in some of the previous DFT+ U calculations, the system was not fully converged to its ground state. The high Eu concentration of Eu (i.e., small supercell sizes) in some calculations may have also introduced strong spurious defect-defect interaction; as a result, the physics at the dilute limit could not be captured properly.

Masago et al. [41–44] reported the electronic structure and energetics of (Eu,Mg)- and (Eu,Mg,O)-doped GaN. Specifically, they investigated the following defect configurations using DFT calculations within GGA: $\text{Eu}_{\text{Ga}}\text{-Eu}_{\text{Ga}}$, $\text{Eu}_{\text{Ga}}\text{-Mg}_{\text{Ga}}\text{-Eu}_{\text{Ga}}$, and $\text{Eu}_{\text{Ga}}\text{-O}_{\text{N}}\text{-Mg}_{\text{Ga}}\text{-Eu}_{\text{Ga}}$, all involving a pair of Eu_{Ga} defects. We do not consider these defect complexes in our current work as they are not relevant to the physics we are investigating.

In short, given the known shortcomings of semilocal functionals such as LDA/GGA [45, 72], care should be taken, however, when interpreting the results. Also note that, in addition to the issue with the electronic structure (including the so-called “band-gap problem”), DFT and DFT+ U calculations based on LDA/GGA are known to provide a poor description of the structure and hence the energetics of defects, even simple native defects [73].

-
- [1] K. O'Donnell and V. Dierolf, eds., *Rare Earth Doped III-Nitrides for Optoelectronic and Spintronic Applications*, Topics in Applied Physics, Vol. 124 (Springer, Dordrecht, 2010).
- [2] Y. Fujiwara and V. Dierolf, Present understanding of Eu luminescent centers in Eu-doped GaN grown by organometallic vapor phase epitaxy, *Jpn. J. Appl. Phys.* **53**, 05FA13 (2014).
- [3] B. Mitchell, V. Dierolf, T. Gregorkiewicz, and Y. Fujiwara, Perspective: Toward efficient GaN-based red light emitting diodes using europium doping, *J. Appl. Phys.* **123**, 160901 (2018).
- [4] Z. Fleischman, C. Munasinghe, A. J. Steckl, A. Wakahara, J. Zavada, and V. Dierolf, Excitation pathways and efficiency of Eu ions in GaN by site-selective spectroscopy, *Appl. Phys. B* **97**, 607 (2009).
- [5] I. S. Roqan, K. P. O'Donnell, R. W. Martin, P. R. Edwards, S. F. Song, A. Vantomme, K. Lorenz, E. Alves, and M. Boćkowski, Identification of the prime optical center in GaN:Eu³⁺, *Phys. Rev. B* **81**, 085209 (2010).
- [6] K. Lorenz, E. Alves, I. S. Roqan, K. P. O'Donnell, A. Nishikawa, Y. Fujiwara, and M. Boćkowski, Lattice site location of optical centers in GaN:Eu light emitting diode material grown by organometallic vapor phase epitaxy, *Appl. Phys. Lett.* **97**, 111911 (2010).
- [7] K. P. O'Donnell, I. S. Roqan, K. Wang, K. Lorenz, E. Alves, and M. Boćkowski, The photoluminescence/excitation (PL/E) spectroscopy of Eu-implanted GaN, *Opt. Mater.* **33**, 1063 (2011).
- [8] N. Woodward, A. Nishikawa, Y. Fujiwara, and V. Dierolf, Site and sample dependent electron-phonon coupling of Eu ions in epitaxial-grown GaN layers, *Opt. Mater.* **33**, 1050 (2011).
- [9] N. Woodward, J. Poplawsky, B. Mitchell, A. Nishikawa, Y. Fujiwara, and V. Dierolf, Excitation of Eu³⁺ in gallium nitride epitaxial layers: Majority versus trap defect center, *App. Phys. Lett.* **98**, 011102 (2011).
- [10] R. Wakamatsu, D. Lee, A. Koizumi, V. Dierolf, and Y. Fujiwara, Luminescence properties of Eu-doped GaN under resonant excitation and quantitative evaluation of luminescent sites, *J. Appl. Phys.* **114**, 043501 (2013).
- [11] B. Mitchell, J. Poplawsky, D. Lee, A. Koizumi, Y. Fujiwara, and V. Dierolf, The role of donor-acceptor pairs in the excitation of Eu-ions in GaN:Eu epitaxial layers, *J. Appl. Phys.* **115**, 204501 (2014).
- [12] D. Timmerman, B. Mitchell, S. Ichikawa, J. Tatebayashi, M. Ashida, and Y. Fujiwara, Excitation Efficiency and Limitations of the Luminescence of Eu³⁺ Ions in GaN, *Phys. Rev. Appl.* **13**, 014044 (2020).
- [13] T. Maruyama, S. Morishima, H. Bang, K. Akimoto, and Y. Nanishi, Valence transition of Eu ions in GaN near the surface, *J. Cryst. Growth* **237-239**, 1167 (2002).
- [14] M. Hashimoto, A. Yanase, R. Asano, H. Tanaka, H. Bang, K. Akimoto, and H. Asahi, Magnetic Properties of Eu-Doped GaN Grown by Molecular Beam Epitaxy, *Jpn. J. Appl. Phys.* **42**, L1112 (2003).
- [15] H. Tanaka, M. Hashimoto, S. Emura, A. Yanase, R. Asano, Y.-K. Zhou, H. Bang, K. Akimoto, T. Honma, N. Umesaki, and H. Asahi, Magnetic properties of the rare-earth-doped semiconductor GaEuN, *phys. status solidi (c)* **0**, 2864 (2003).
- [16] J. H. Kim and P. H. Holloway, Room-temperature photoluminescence and electroluminescence properties of sputter-grown gallium nitride doped with europium, *J. Appl. Phys.* **95**, 4787 (2004).
- [17] J. Hite, G. T. Thaler, R. Khanna, C. R. Abernathy, S. J. Pearton, J. H. Park, A. J. Steckl, and J. M. Zavada, Optical and magnetic properties of Eu-doped GaN, *App. Phys. Lett.* **89**, 132119 (2006).
- [18] V. Mahalingam, M. Tan, P. Munusamy, J. B. Gilroy, M. Raudsepp, and F. C. J. M. van Veggel, Bright Blue Photo- and Electroluminescence from Eu²⁺-Doped GaN/SiO₂ Nanocomposites, *Adv. Funct. Mater.* **17**, 3462 (2007).
- [19] B. Mitchell, A. Koizumi, T. Nunokawa, R. Wakamatsu, D. Lee, Y. Saitoh, D. Timmerman, Y. Kuboshima, T. Mogi, S. Higashi, K. Kikukawa, H. Ofuchi, T. Honma, and Y. Fujiwara, Synthesis and characterization of a liquid Eu precursor (EuCp₂^{pm}) allowing for valence control of Eu ions doped into GaN by organometallic vapor phase epitaxy, *Mater. Chem. Phys.* **193**, 140 (2017).
- [20] T. Nunokawa, Y. Fujiwara, Y. Miyata, N. Fujimura, T. Sakurai, H. Ohta, A. Masago, H. Shinya, T. Fukushima, K. Sato, and H. Katayama-Yoshida, Valence states and the magnetism of Eu ions in Eu-doped GaN, *J. Appl. Phys.* **127**, 083901 (2020).
- [21] B. Mitchell, D. Timmerman, J. Poplawsky, W. Zhu, D. Lee, R. Wakamatsu, J. Takatsu, M. Matsuda, W. Guo, K. Lorenz, E. Alves, A. Koizumi, V. Dierolf, and Y. Fujiwara, Utilization of native oxygen in Eu(RE)-doped GaN for enabling device compatibility in optoelectronic applications, *Sci. Rep.* **6**, 18808 (2016).
- [22] W. Zhu, B. Mitchell, D. Timmerman, A. Uedono, A. Koizumi, and Y. Fujiwara, Enhanced photo/electroluminescence properties of Eu-doped GaN through optimization of the growth temperature and Eu related defect environment, *APL Mater.* **4**, 056103 (2016).
- [23] Y. Takagi, T. Suwa, H. Sekiguchi, H. Okada, and A. Wakahara, Effect of Mg codoping on Eu³⁺ luminescence in GaN grown by ammonia molecular beam epitaxy, *App. Phys. Lett.* **99**, 171905 (2011).
- [24] D. Lee, A. Nishikawa, Y. Terai, and Y. Fujiwara, Eu luminescence center created by Mg codoping in Eu-doped GaN, *App. Phys. Lett.* **100**, 171904 (2012).
- [25] A. Wakahara, H. Sekiguchi, H. Okada, and Y. Takagi, Current status for light-emitting diode with Eu-doped GaN active layer grown by MBE, *J. Lumin.* **132**, 3113 (2012).
- [26] H. Sekiguchi, Y. Takagi, T. Otani, H. Okada, and A. Wakahara, Emission enhancement mechanism of GaN:Eu by Mg codoping, *J. Appl. Phys.* **113**, 013105 (2013).
- [27] H. Sekiguchi, M. Sakai, T. Kamada, H. Tateishi, A. Syouji, and A. Wakahara, Optical sites in Eu- and Mg-codoped GaN grown by NH₃-source molecular beam epitaxy, *App. Phys. Lett.* **109**, 151106 (2016).
- [28] R. Wang, A. J. Steckl, E. E. Brown, U. Hommerich, and J. M. Zavada, Effect of Si codoping on Eu³⁺ luminescence in GaN, *J. Appl. Phys.* **105**, 043107 (2009).
- [29] K. P. O'Donnell, P. R. Edwards, M. J. Kappers, K. Lorenz, E. Alves, and M. Boćkowski, Europium-doped

- GaN(Mg): beyond the limits of the light-emitting diode, *phys. status solidi c* **11**, 662 (2014).
- [30] K. P. O'Donnell, P. R. Edwards, M. Yamaga, K. Lorenz, M. J. Kappers, and M. Boćkowski, Crystalfield symmetries of luminescent Eu^{3+} centers in GaN: The importance of the 5D_0 to 7F_1 transition, *App. Phys. Lett.* **108**, 022102 (2016).
- [31] A. K. Singh, K. P. O'Donnell, P. R. Edwards, K. Lorenz, M. J. Kappers, and M. Boćkowski, Hysteretic photochromic switching of Eu-Mg defects in GaN links the shallow transient and deep ground states of the Mg acceptor, *Sci. Rep.* **7**, 41982 (2017).
- [32] D. Cameron, K. P. O'Donnell, P. R. Edwards, M. Peres, K. Lorenz, M. J. Kappers, and M. Boćkowski, Acceptor state anchoring in gallium nitride, *App. Phys. Lett.* **116**, 102105 (2020).
- [33] J.-S. Filhol, R. Jones, M. J. Shaw, and P. R. Briddon, Structure and electrical activity of rare-earth dopants in GaN, *Appl. Phys. Lett.* **84**, 2841 (2004).
- [34] A. Svane, N. E. Christensen, L. Petit, Z. Szotek, and W. M. Temmerman, Electronic structure of rare-earth impurities in GaAs and GaN, *Phys. Rev. B* **74**, 165204 (2006).
- [35] S. Sanna, W. G. Schmidt, T. Frauenheim, and U. Gerstmann, Rare-earth defect pairs in GaN: LDA+ U calculations, *Phys. Rev. B* **80**, 104120 (2009).
- [36] C. N. Ouma and W. E. Meyer, *Ab initio* study of metastability of Eu^{3+} defect complexes in GaN, *Physica B: Condens. Matter* **439**, 141 (2014).
- [37] B. Mitchell, N. Hernandez, D. Lee, A. Koizumi, Y. Fujiwara, and V. Dierolf, Charge state of vacancy defects in Eu-doped GaN, *Phys. Rev. B* **96**, 064308 (2017).
- [38] S. Goumri-Said and M. B. Kanoun, Electronic structure and magnetism of Eu-doped GaN: first-principles study based on LDA+ U , *J. Phys. D: Appl. Phys.* **41**, 035004 (2008).
- [39] H. Su, T. Wang, Z. Hou, H. Liu, C. Liu, and Y. Li, Electronic and magnetic properties of defect complexes in Eu-doped GaN: First-principles calculations, *Physica B: Condens. Matter* **542**, 1 (2018).
- [40] A. V. B. Cruz, P. P. Shinde, V. Kumar, and J. M. Zavada, Energetics and electronic structure of GaN codoped with Eu and Si, *Phys. Rev. B* **85**, 045203 (2012).
- [41] A. Masago, T. Fukushima, K. Sato, and H. Katayama-Yoshida, Luminescent centers in GaN codoped with Eu and Mg: Calculation on density functional theory, *Jpn. J. Appl. Phys.* **53**, 061001 (2014).
- [42] A. Masago, T. Fukushima, K. Sato, and H. Katayama-Yoshida, Efficient luminescent center by codoping (Eu,Mg,O) into GaN, *Appl. Phys. Express* **7**, 071005 (2014).
- [43] A. Masago, T. Fukushima, K. Sato, and H. Katayama-Yoshida, Computational nano-materials design for circularly polarized luminescence in (Eu,Mg,O)-codoped GaN, *Appl. Phys. Express* **7**, 121002 (2014).
- [44] A. Masago, M. Uemoto, T. Fukushima, K. Sato, and H. Katayama-Yoshida, Computational materials design for efficient red luminescence: InGaN codoped with Eu and the donor-acceptor pair of Mg and O, *Jpn. J. Appl. Phys.* **56**, 021001 (2017).
- [45] C. Freysoldt, B. Grabowski, T. Hickel, J. Neugebauer, G. Kresse, A. Janotti, and C. G. Van de Walle, First-principles calculations for point defects in solids, *Rev. Mod. Phys.* **86**, 253 (2014).
- [46] See the Appendices for more results and further discussion.
- [47] J. Heyd, G. E. Scuseria, and M. Ernzerhof, Hybrid functionals based on a screened Coulomb potential, *J. Chem. Phys.* **118**, 8207 (2003).
- [48] K. Hoang, First-principles identification of defect levels in Er-doped GaN, *Phys. Status Solidi RRL* **10**, 915 (2016).
- [49] C. G. Van de Walle and J. Neugebauer, First-principles calculations for defects and impurities: Applications to III-nitrides, *J. Appl. Phys.* **95**, 3851 (2004).
- [50] C. Freysoldt, J. Neugebauer, and C. G. Van de Walle, Fully *Ab Initio* Finite-Size Corrections for Charged-Defect Supercell Calculations, *Phys. Rev. Lett.* **102**, 016402 (2009).
- [51] C. Freysoldt, J. Neugebauer, and C. G. Van de Walle, Electrostatic interactions between charged defects in supercells, *phys. status solidi (b)* **248**, 1067 (2011).
- [52] K. Hoang and M. D. Johannes, Defect physics in complex energy materials, *J. Phys.: Condens. Matter* **30**, 293001 (2018).
- [53] G. Kresse and D. Joubert, From ultrasoft pseudopotentials to the projector augmented-wave method, *Phys. Rev. B* **59**, 1758 (1999).
- [54] G. Kresse and J. Furthmüller, Efficient iterative schemes for ab initio total-energy calculations using a plane-wave basis set, *Phys. Rev. B* **54**, 11169 (1996).
- [55] M. Hacene, A. Anciaux-Sedrakian, X. Rozanska, D. Klahr, T. Guignon, and P. Fleurat-Lessard, Accelerating VASP electronic structure calculations using graphic processing units, *J. Comput. Chem.* **33**, 2581 (2012).
- [56] M. Hutchinson and M. Widom, VASP on a GPU: Application to exact-exchange calculations of the stability of elemental boron, *Comput. Phys. Commun.* **183**, 1422 (2012).
- [57] K. Hoang, Hybrid density functional study of optically active Er^{3+} centers in GaN, *Phys. Status Solidi RRL* **9**, 722 (2015).
- [58] H. Schulz and K. H. Thiemann, Crystal structure refinement of AlN and GaN, *Solid State Commun.* **23**, 815 (1977).
- [59] C. H. Park and D. J. Chadi, Stability of deep donor and acceptor centers in GaN, AlN, and BN, *Phys. Rev. B* **55**, 12995 (1997).
- [60] C. G. Van de Walle, DX -center formation in wurtzite and zinc-blende $\text{Al}_x\text{Ga}_{1-x}\text{N}$, *Phys. Rev. B* **57**, R2033 (1998).
- [61] L. Gordon, J. L. Lyons, A. Janotti, and C. G. Van de Walle, Hybrid functional calculations of DX centers in AlN and GaN, *Phys. Rev. B* **89**, 085204 (2014).
- [62] G. B. Wilson-Short, A. Janotti, K. Hoang, A. Peles, and C. G. Van de Walle, First-principles study of the formation and migration of native defects in NaAlH_4 , *Phys. Rev. B* **80**, 224102 (2009).
- [63] K. Hoang and M. Johannes, Tailoring Native Defects in LiFePO_4 : Insights from First-Principles Calculations, *Chem. Mater.* **23**, 3003 (2011).
- [64] S. Lany and A. Zunger, Dual nature of acceptors in GaN and ZnO: The curious case of the shallow Mg_{Ga} deep state, *App. Phys. Lett.* **96**, 142114 (2010).
- [65] J. L. Lyons, A. Janotti, and C. G. Van de Walle, Shallow versus Deep Nature of Mg Acceptors in Nitride Semiconductors, *Phys. Rev. Lett.* **108**, 156403 (2012).
- [66] J. P. Perdew, K. Burke, and M. Ernzerhof, Generalized gradient approximation made simple, *Phys. Rev. Lett.* **77**, 3865 (1996).

- [67] J. W. Mayer and S. S. Lau, *Electronic Materials Science: For Integrated Circuits in Si and GaAs* (MacMillan Publishing, New York, 1990) p. 161.
- [68] T. Inaba, T. Kojima, G. Yamashita, E. Matsubara, B. Mitchell, R. Miyagawa, O. Eryu, J. Tatebayashi, M. Ashida, and Y. Fujiwara, Quantitative study of energy-transfer mechanism in Eu,O-codoped GaN by time-resolved photoluminescence spectroscopy, *J. Appl. Phys.* **123**, 161419 (2018).
- [69] S. L. Dudarev, G. A. Botton, S. Y. Savrasov, C. J. Humphreys, and A. P. Sutton, Electron-energy-loss spectra and the structural stability of nickel oxide: An LSDA+*U* study, *Phys. Rev. B* **57**, 1505 (1998).
- [70] Q. Yan, A. Janotti, M. Scheffler, and C. G. Van de Walle, Role of nitrogen vacancies in the luminescence of Mg-doped GaN, *Appl. Phys. Lett.* **100**, 142110 (2012).
- [71] J. L. Lyons and C. G. Van de Walle, Computationally predicted energies and properties of defects in GaN, *npj Comput. Mater.* **3**, 12 (2017).
- [72] W. R. L. Lambrecht, Electronic structure of magnetic impurities and defects in semiconductors: a guide to the theoretical models, in *Rare Earth and Transition Metal Doping of Semiconductor Materials: Synthesis, Magnetic Properties and Room Temperature Spintronics*, Woodhead Publishing Series in Electronic and Optical Materials, Vol. 87, edited by V. Dierolf, I. T. Ferguson, and J. M. Zavada (Elsevier, Amsterdam, 2016) pp. 43–101.
- [73] J. L. Lyons, A. Alkauskas, A. Janotti, and C. G. Van de Walle, First-principles theory of acceptors in nitride semiconductors, *phys. status solidi (b)* **252**, 900 (2015).